Wall-Modeled Large-Eddy Simulation of High-Speed Turbulent Flows with an Immersed Boundary Method

W. van Noordt[1], S. Ganju[2], C. Brehm[2,3]

[1]*Department of Engineering Science*, University of Oxford

[2]*Department of Aerospace Engineering*, University of Maryland

[3]*Department of Mechanical Engineering*, University of Kentucky

Funded by Hypersonic Vehicle Simulation Institute with **Dr. Russ Cummings** as Program Director.

Advanced Modeling and Simulation Seminar Series – NASA Ames Research Center, Aug 19 2021

Background

- Increasing interest in high-speed flows in the last few years, especially due to DoD relevance and space exploration
  - Rapid response and deployment capabilities
  - Space access and re-entry

- Combination of many relevant physical phenomena
  - Real-gas effects, shocks, SWBLI, large transition regions

- Challenges for hypersonic turbulence modeling (in addition to those from the low-speed regime):
  - Accurate prediction of regions with mixed laminar, transitional and turbulent flows
  - High temperature and compressibility effects, e.g., real gas effects
  - Aerodynamic heating
  - + all remaining challenges from the low-speed regime carry over, e.g., separation prediction, etc.
  - Limited development and testing of hybrid RANS-LES and WMLES approaches for high-speed flow problems

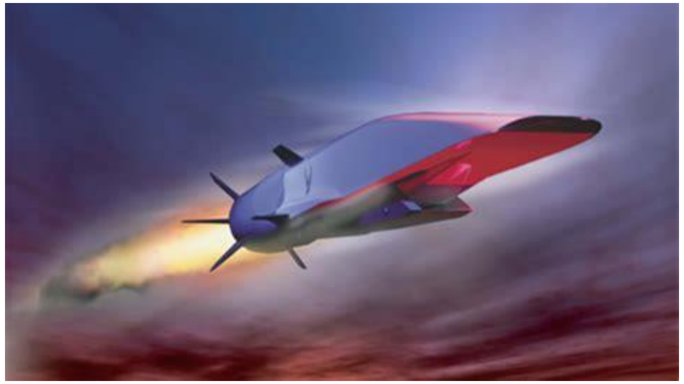

Artist's concepts of hypersonic cruise hardware.

High-Fidelity Simulations

- Coming years will see a substantial increase in the use of hybrid RANS-LES (HRLM) and wall-modeled LES (WMLES) methods for industrial applications due to:
  - Increased availability of HPC resources leading to faster turn-around times ($\sim$ 24-48 hours)
  - Complex hypersonic flow phenomena, e.g., transition, turbulent separation, etc., cannot be predicted with current state-of-the-art RANS methods

- High-fidelity simulations for practical turbulent flow scenarios (high-Re) are computationally expensive[1]
  - $(N_x N_t)_{DNS} \sim Re_{L_x}^{2.91}$, $(N_x N_t)_{WRLES} \sim {Re_{L_x}}^{2.72}$

- WMLES provides a viable alternative for high-fidelity simulations at reasonable cost
  - $(N_x N_t)_{WMLES} \sim Re_{L_x}^{1.14}$
  - Wall modeling allows for more fully-automated grid generation due to coarse grid resolution near the solid boundary

- Numerous challenges in LES/WMLES of high-speed flows, grid sensitivity

[1]Yang, X. I. A., & Griffin, K. P. (2021). Grid-point and time-step requirements for direct numerical simulation and large-eddy simulation. *Physics of Fluids*, *33*(1), 015108.

Immersed Boundary Methods

- Allow practitioners to side-step costly mesh generation process
  - Reduce mesh generation process to a small number of parameters, otherwise fully automated

- Arbitrary geometry is superimposed over a uniformly Cartesian grid
  - Apply a boundary closure rule to governing equations
  - Block-structure allows for simple AMR to resolve structures near boundary
- Simple, structured data layout with fixed spacing has favorable characteristics for HPC compared with e.g. unstructured approach

- Challenges
  - Limited to small aspect ratios
  - Numerical instability at boundaries
  - Reduction of order-of-accuracy at boundaries

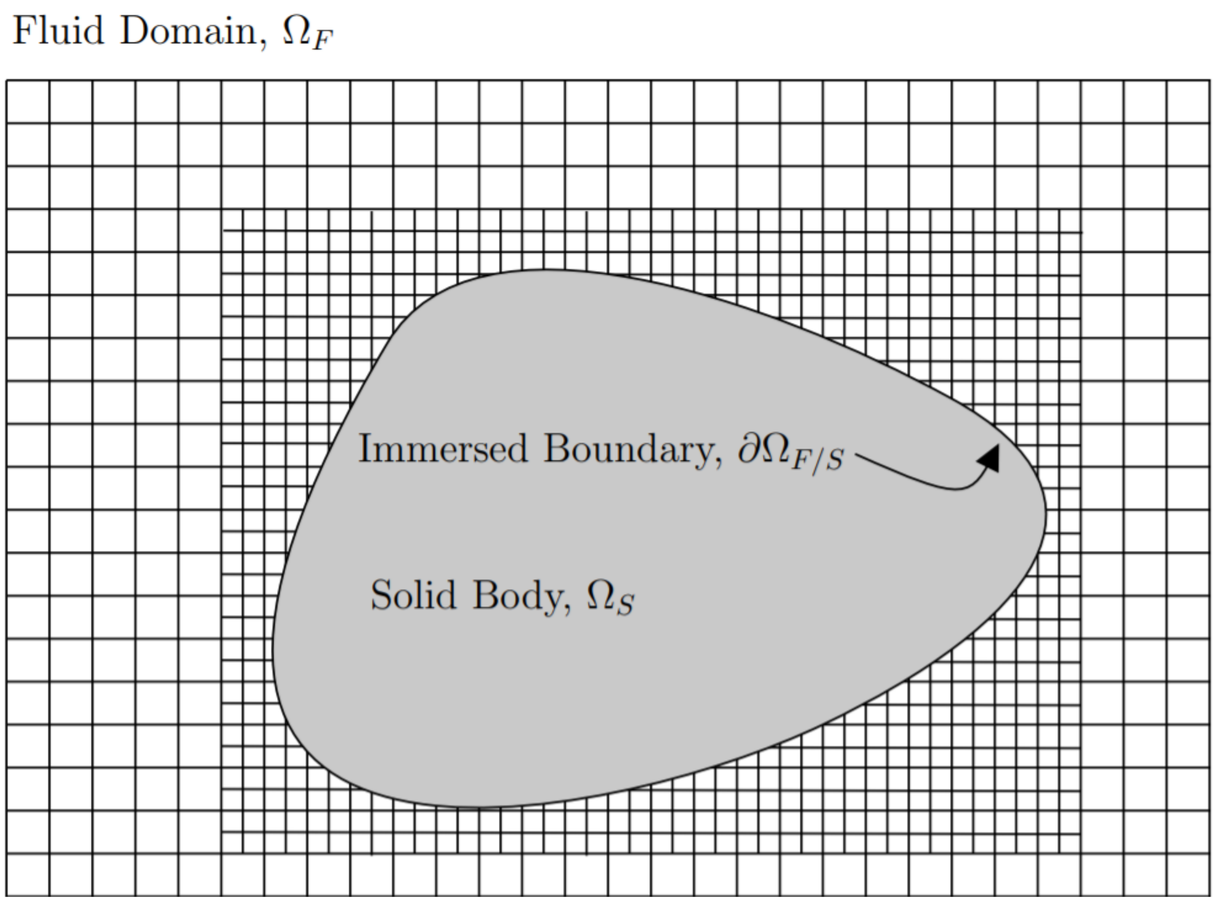

Example of a solid object immersed in a Cartesian Grid

Numerical Methods for High-Fidelity Turbulence Modeling

- Conflicting requirements on numerical methods for WMLES of hypersonic flows:
  - Non-dissipative
  - Robust at solution discontinuities
- IBM-WMLES has additional conflicting requirements at boundaries:
  - IB treatment typically suffers numerical instabilities
  - Under-resolution of WMLES grid can give rise to discontinuities at IB
  - Strong stability requirements on inherently unstable numerical method
- Numerical methods must be solution-adaptive while maintaining efficient implementation
- Importance of secondary properties
  - Discrete kinetic energy conservation
  - Discrete entropy conservation

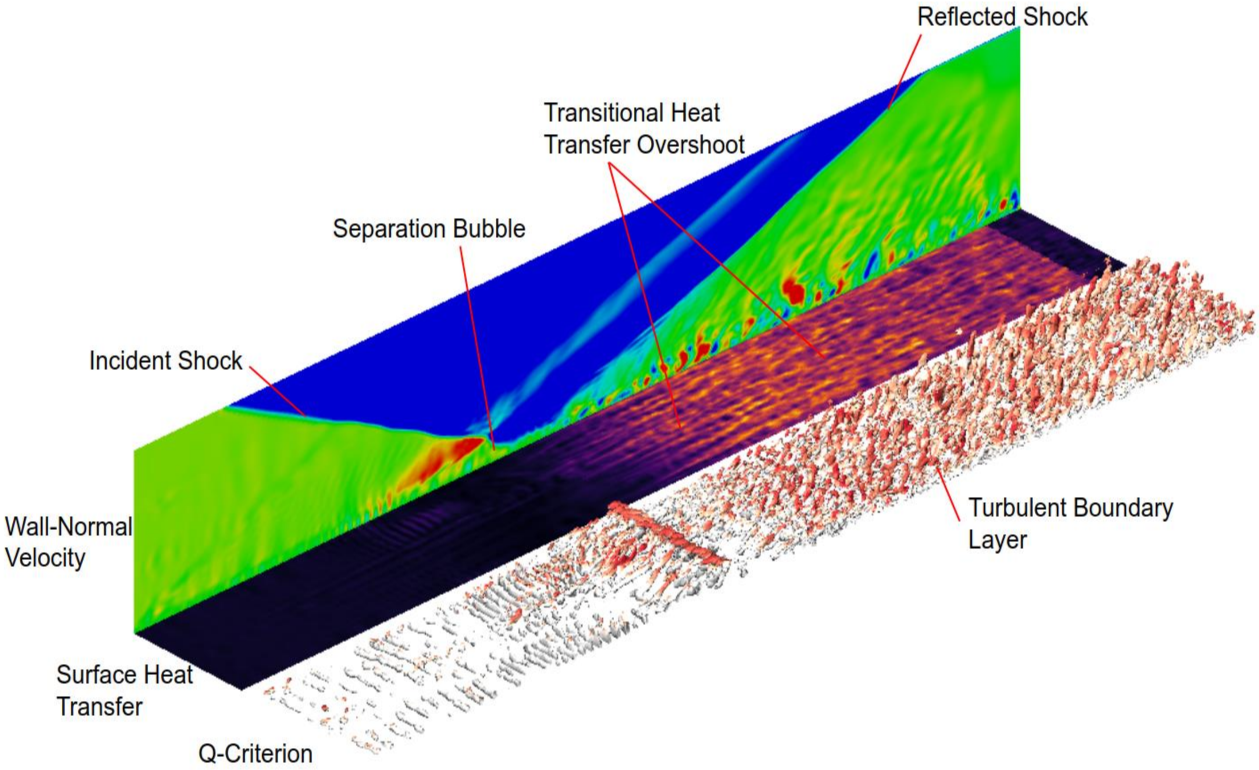

Hypersonic shock-wave boundary-layer interaction (SWBLI) highlights a number of challenging phenomena

Numerical Scheme for WMLES

Numerical scheme must be non-dissipative and provide sufficient dissipation to handle flow discontinuities:

$$\hat{f}_{i+1/2} = (1-\alpha)\hat{f}^{Cent}_{i+1/2} + \alpha\hat{f}^{Diss}_{i+1/2}$$

Interior

- *Cent*: Fourth-order, centered, kinetic energy and entropy preserving (KEEP) scheme[1,2]
- *Diss*: Third-order WENO scheme

Boundary Closure

- Irregular boundary closure has a strong effect on solution accuracy
- *Cent*: Reduce to 2nd-order at the wall
  - *For one irregular point treatment higher-order (>2) is challenging*
- *Diss*: Developed third-order boundary closure to be consistent with interior scheme
  - *Irregular reconstruction and smoothness operators follow approach in Brehm 2017[3]*

Inviscid Taylor-Green vortex, kinetic energy

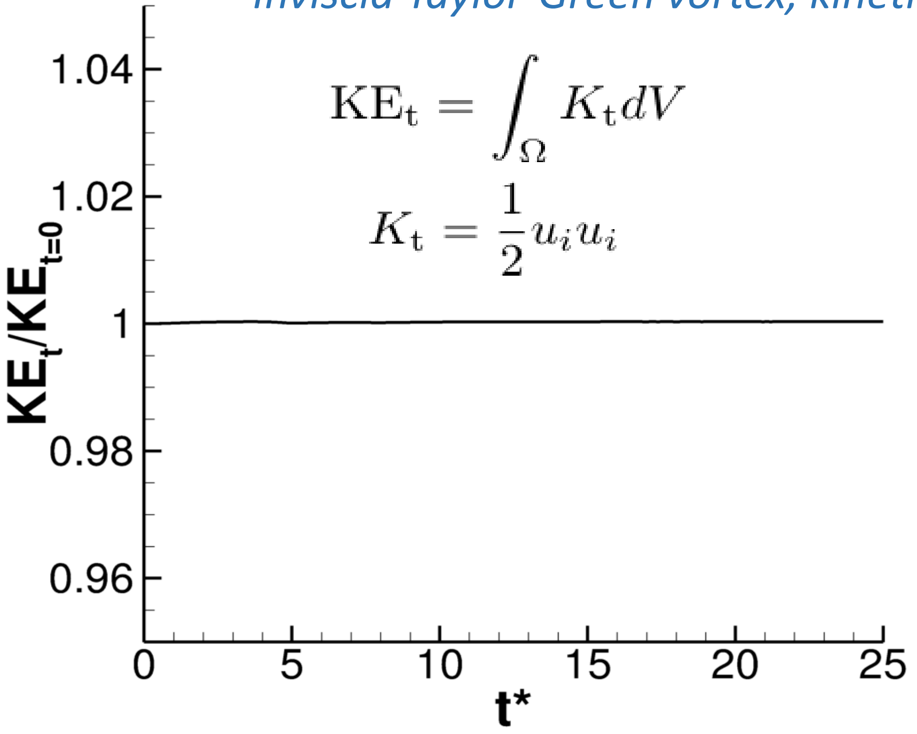

[1]Kuya, Y., Totani, K., & Kawai, S. (2018). Kinetic energy and entropy preserving schemes for compressible flows by split convective forms. *Journal of Computational Physics*, *375*, 823–853.

[2]Totani, K., Kuya, Y., & Kawai, S. (2019). High-order-accurate kinetic energy and entropy preserving schemes on curvilinear meshes. In *AIAA Scitech 2019 Forum*.

[3]Brehm, (2017), On consistent boundary closures for compact finite-difference WENO schemes, Journal of Computational Physics, 334, 573-581.

Numerical Methods – WENO IB Closure

- Conservative Finite Difference Operator:

$$\frac{\partial f}{\partial x} = \frac{1}{\Delta x}\left(h_{i+1/2} - h_{i-1/2}\right) = \frac{1}{\Delta x}\left(\hat{f}_{i+1/2} - \hat{f}_{i-1/2}\right) + \mathcal{O}(\Delta x^{2n-1})$$

- Scheme relies on error cancellation
  - Numerical flux derivative at x_i: $$\left.\frac{\partial f}{\partial x}\right|_{x=x_i} = \frac{h_{i+1/2} - h_{i-1/2}}{\Delta x} \approx \frac{\hat{f}_{i+1/2} - \hat{f}_{i-1/2}}{\Delta x} \qquad (1)$$
  - Truncation error obtaining flux at $x_{i+1/2}$: $$\hat{f}_{i+1/2} = h_{i+1/2} - A\left.\frac{\partial^3 f}{\partial x^3}\right|_{x=x_i}\Delta x^3 \quad \text{(scheme A)} \qquad (2)$$
  - Truncation error obtaining flux at $x_{i-1/2}$: $$\hat{f}_{i-1/2} = h_{i-1/2} - B\left.\frac{\partial^3 f}{\partial x^3}\right|_{x=x_i}\Delta x^3 \quad \text{(scheme B)} \qquad (3)$$
  - Substituting (2) and (3) in (1) leads to: $$\left.\frac{\partial f}{\partial x}\right|_{x=x_i} = \frac{h_{i+1/2}-h_{i-1/2}}{\Delta x} - (B-A)\left.\frac{\partial^3 f}{\partial x^3}\right|_{x=x_i}\Delta x^2 + O(\Delta x^3)$$

➢ *To recover formal order-of-accuracy match not only order but also leading term of truncation error*

Numerical Methods – WENO IB Closure

- Introduce weights on candidate FD stencils:

$$\frac{\partial f}{\partial x} = \sum_{l} \omega_l \sum_{k \in S_1} c_k \hat{f}_{k+1/2}$$

- Weights computed according to the smoothness of the solution on stencil:

$$\beta_l = \sum_{j=1}^{n-1} \Delta x^{2j-1} \int_{x_{l,min}}^{x_{l,max}} \left(\frac{d\hat{f}_k}{dx^j}\right)^2 dx, \qquad \omega_l = \frac{c_l}{(\beta_l + \varepsilon)^p}$$

- Irregular smoothness indicator avoids the use of ghost cell information → avoid erroneous stencil switching
- WENO procedure necessary for flows with shocks
- Smoothness can be defined for a number of different variables (primitive/conservative/characteristic/…)

Immersed Boundary Method and Wall Model Coupling

Projected Sampling Points from Face Centroid | *Flow Field Interpolation* | *On-Surface Face-Neighbor Interpolation* | *Computation of Boundary Conditions via Extrapolation*

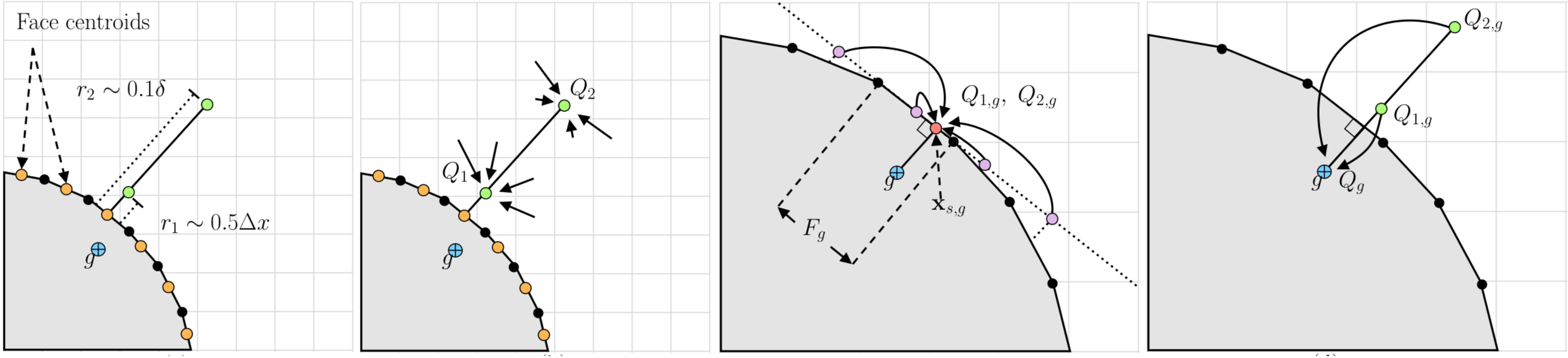

- No-slip wall boundary condition is not imposed
  - Tangential velocity is extrapolated to minimize effects of dissipation near the wall
  - Zero-penetration enforced through wall-normal velocity
  - Neumann boundary condition for pressure/temperature
- On-surface interpolation preserves spatial locality through ghost cells

WENO IB Closure – *Stability Analysis*

- Linear stability analysis performed on current IB closure (optimal stencils)

- Upwind portion of flux shows finite-time stability for large CFL conditions; *modulus of the largest pseudo-eigenvalues reside within stability region for* $\varepsilon = 10^{-3}$

Pseudo-Eigenvalue Spectrum of Upwind IB Closure.

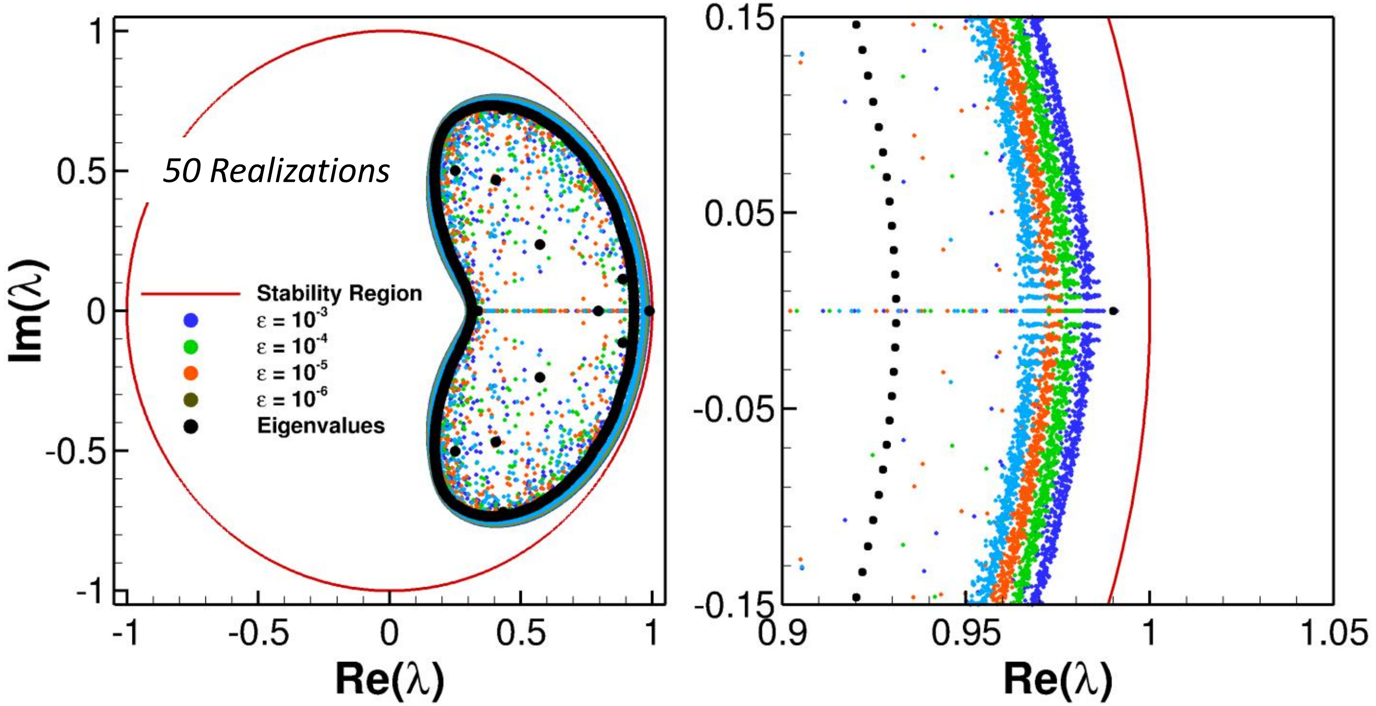

Model Equation: $\frac{\partial u}{\partial t} + a\frac{\partial u}{\partial x} = 0 \rightarrow \frac{\partial \boldsymbol{u}}{\partial t} + a\frac{1}{\Delta x}D\boldsymbol{u} \rightarrow \boldsymbol{u}^{n+1} = A\boldsymbol{u}^n$

Update Matrix: $A = I - \gamma D + \frac{1}{2!}\gamma^2 D^2 - \frac{1}{3!}\gamma^3 D^3 + \frac{1}{4!}\gamma^4 D^4$

Pseudo-spectrum[1]: $dist(\Lambda_\varepsilon\{A\}, S) = O(\varepsilon) \qquad S = \{\omega \in \mathbb{C}: |\omega| \le 1\}$

$$\Lambda_\varepsilon\{A\} = \bigcup_{||M||=\varepsilon} \{\lambda \in \mathbb{C}: \det(\lambda I - A + M) = 0\}$$

[1]Brehm, (2017), On consistent boundary closures for compact finite-difference WENO schemes, Journal of Computational Physics, 334, 573-581.

WENO IB Closure – *Stability Analysis*

- Centered operator spectrally stable, but boundary closure introduces pseudo-spectral instability – add minimal boundary dissipation to stabilize

- Upwind operator introduced at the boundary via blending parameter

$$\alpha_j = e^{-(j+1)}$$

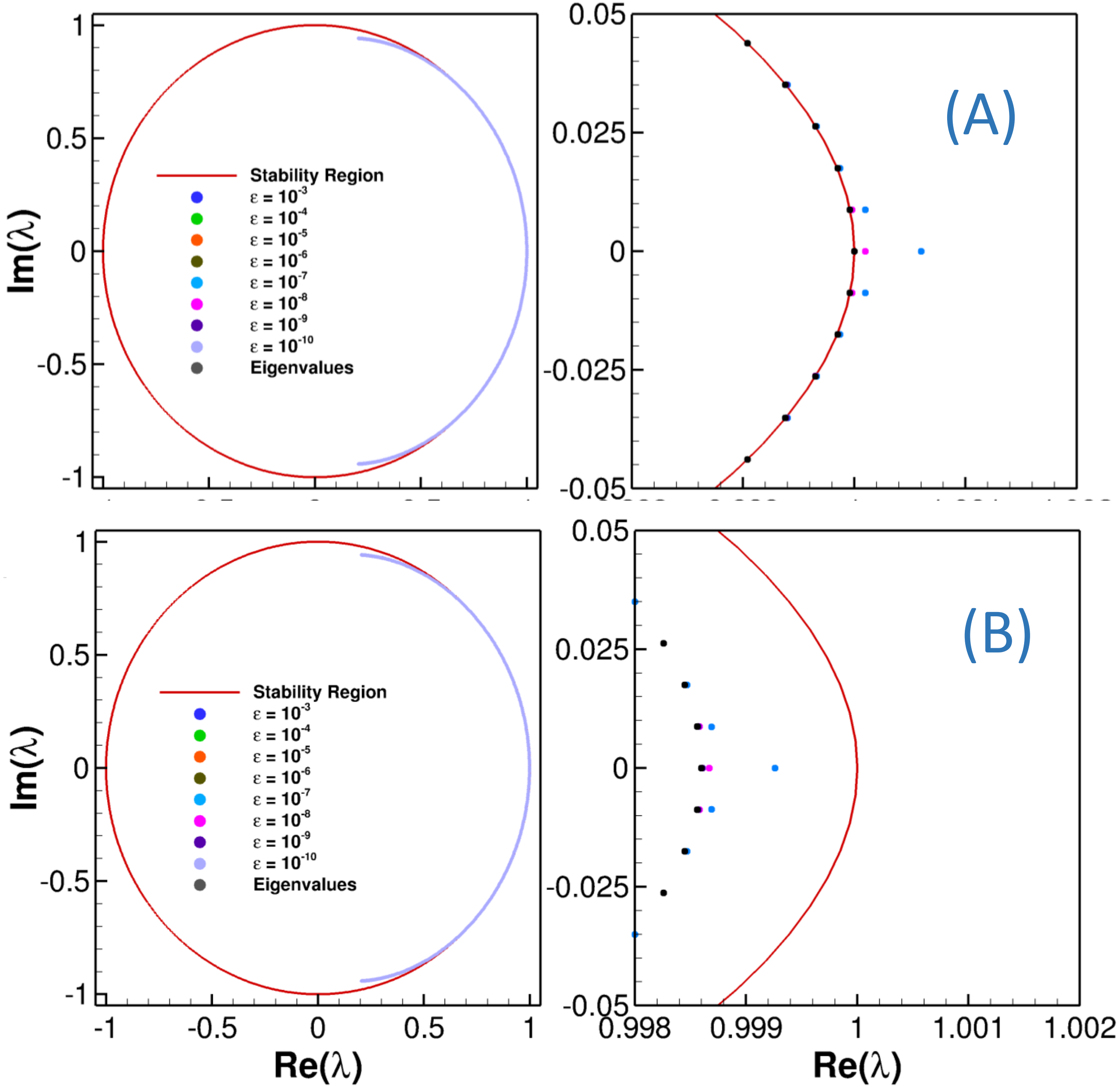

Zoomed view of the critical stability region for (A) centered IB operator and (B) modified IB operator

Numerical Methods – Viscous Discretization

- Conservative discretization of viscous terms is essential for WMLES

$$\frac{\partial \boldsymbol{g}}{\partial x} \approx \frac{\widehat{\boldsymbol{g}}_{i+1/2} - \widehat{\boldsymbol{g}}_{i-1/2}}{\Delta x}$$

- If one of the faces is irregular then truncation error of viscous flux at the half point needs to match
  - Interpolation to face:

$$\phi_{i+1/2,j} = \frac{1}{2}\left(\phi_{i,j} + \phi_{i+1,j}\right) + \frac{1}{8}\Delta x^2 \phi_{xx} + \mathcal{O}(\Delta x^3)$$

  - Derivatives:

$$\left.\frac{\partial \phi}{\partial y}\right|_{i+1/2j} = \frac{1}{2}\left(\frac{\phi_{i+1,j+1} - \phi_{i+1,j-1}}{2\Delta y} + \frac{\phi_{i,j+1} - \phi_{i,j-1}}{2\Delta y}\right) + \frac{1}{6}\Delta y^2 \left.\phi_{yyy}\right|_{i+1/2,j} + \frac{1}{8}\Delta x^2 \left.\phi_{yxx}\right|_{i+1/2,j} + \mathcal{O}(\Delta y^3, \Delta x^3, \Delta x \Delta y^2)$$

$$\left.\frac{\partial \phi}{\partial x}\right|_{i+1/2,j} = \frac{\phi_{i+1,j} - \phi_{i,j}}{\Delta x} - \frac{1}{24}\Delta x^2 \phi_{xxx} + \mathcal{O}(\Delta x^3)$$

  - Matching truncation error at irregular face

$$\mathcal{R}\phi = \sum_{i,j\in J} c_{i,j}\phi_{i,j} + k_1 \Delta x^2 + k_2 \Delta y^2 + \mathcal{O}(\Delta x^3, \Delta x^2 \Delta y, \Delta x \Delta y^2, \Delta y^3), \quad \mathcal{R} \in \left\{1, \frac{\partial}{\partial x}, \frac{\partial}{\partial y}\right\}$$

- Viscous flux on immersed boundary provided by wall model

Irregular Faces in Vicinity of the Boundary

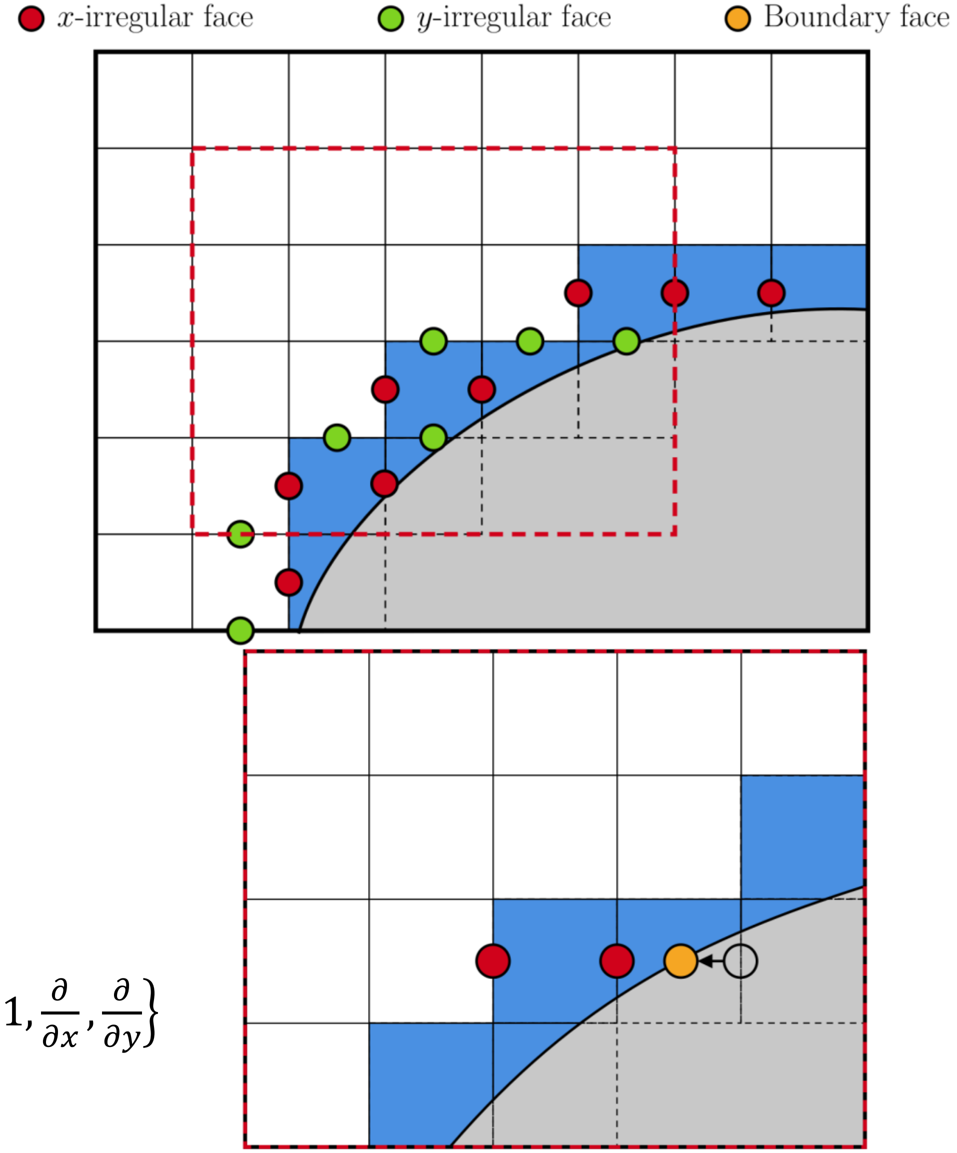

Numerical Methods – Wall Model

- Present method employs simple equilibrium wall model: viscous diffusive equilibrium

$$\frac{d}{dn}\left((\mu + \mu_t)\frac{du}{dn}\right) = 0, \qquad \mu_t = \kappa\mu y^+\left(1 - e^{\frac{y^+}{A^+}}\right)^2$$

- Contribution from aerodynamic heating significant in wall-model layer when $M^2 C_f^{\frac{1}{2}} = O(1)$[1] (significant around $M \cong 3$):

$$\frac{d}{dn}\left((\mu + \mu_t)u\frac{du}{dn} + c_p\left(\frac{\mu}{Pr} + \frac{\mu_t}{\mathrm{Pr_t}}\right)\frac{dT}{dn}\right) = 0$$

- Coupling of flow-field data performed via 3rd-order interpolation operation with matching truncation error

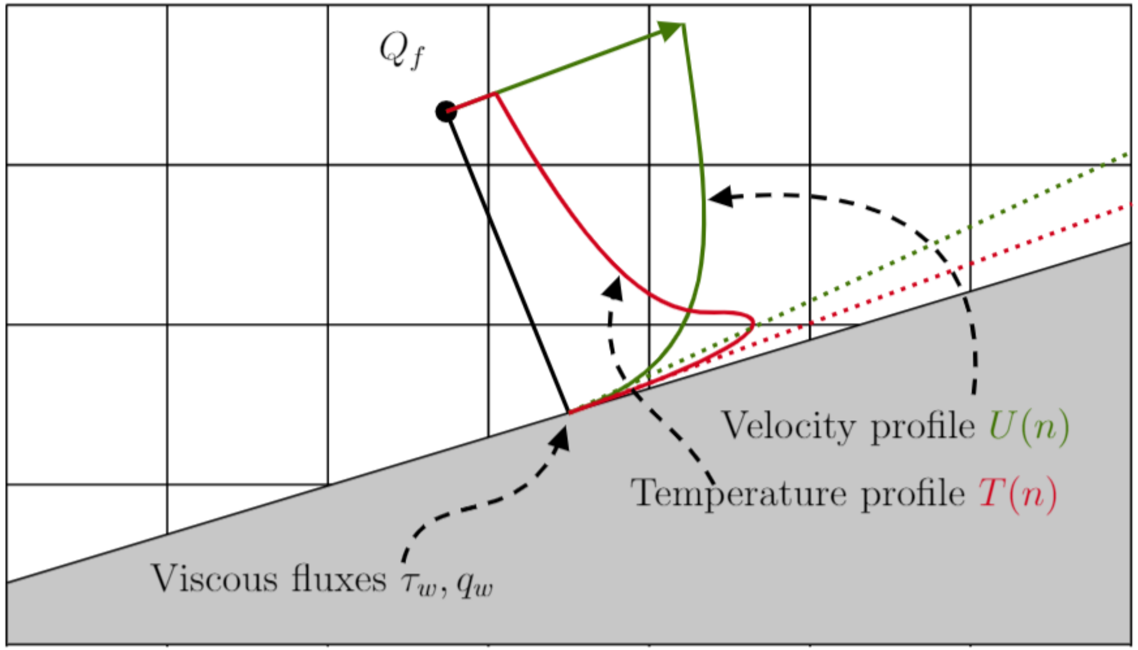

Cartesian Grid WM Coupling

[1] Yang, Urzay, Bose, Moin, (2018), Aerodynamics heating in wall-modeled large-eddy simulation of high-speed flows, AIAA Journal 56, 731-742.

WMLES Simulations – Overview

Total Grid Size	$\Delta x^+ \times \Delta y^+ \times \Delta z^+$	$L_x \times L_y \times L_z$	M_∞	Re_b
1.9M	$270 \times 68 \times 270$	$12.8\delta \times 2\delta \times 4.8\delta$	0.2	125,000

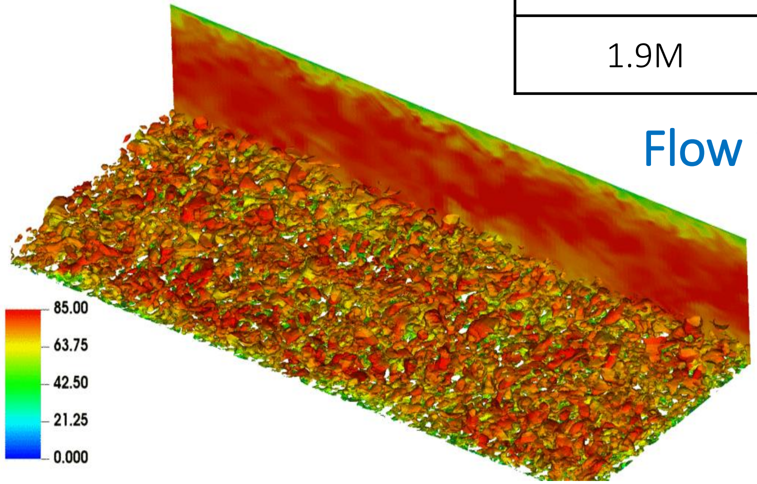

Flow in a turbulent channel at $\mathbf{Re_\tau = 5200}$

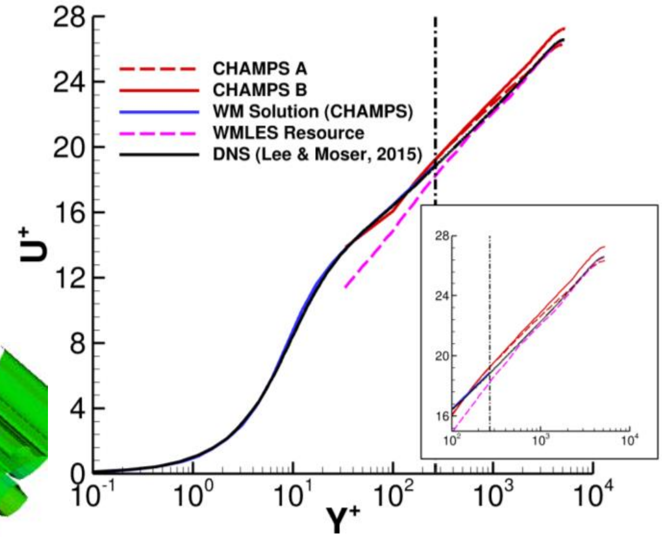

Total Grid Size	M_∞	Re_b
50M	0.2	10^6

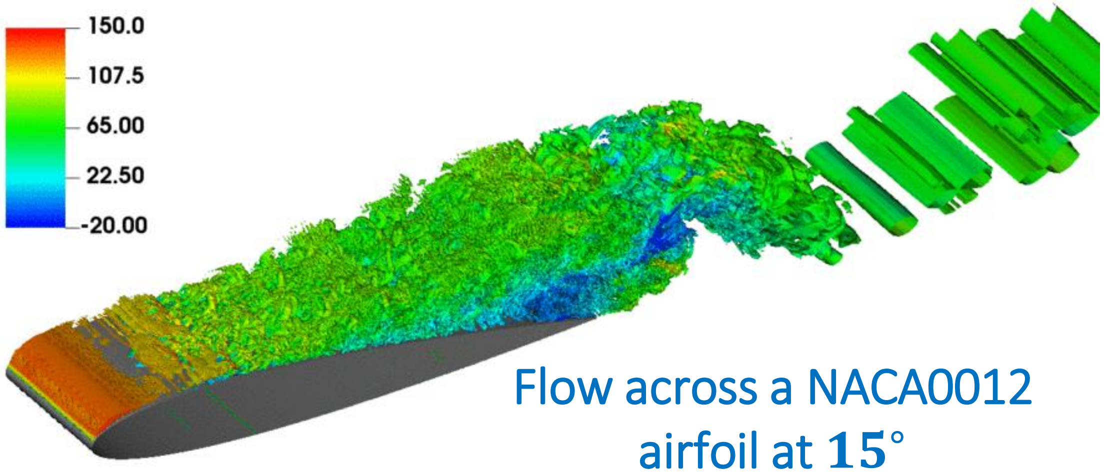

Flow across a NACA0012 airfoil at $\mathbf{15}°$

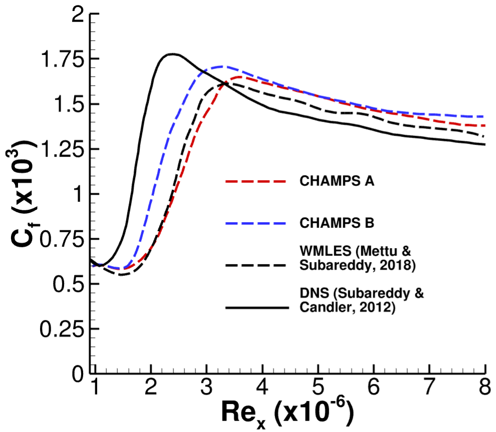

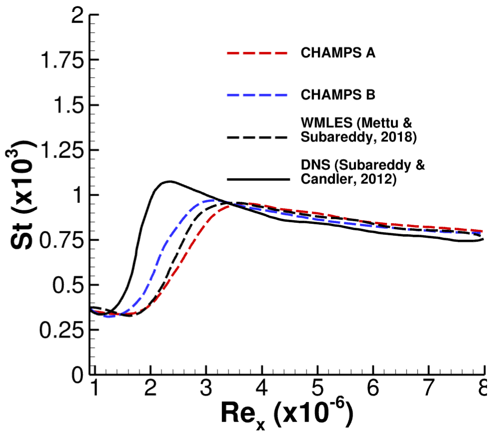

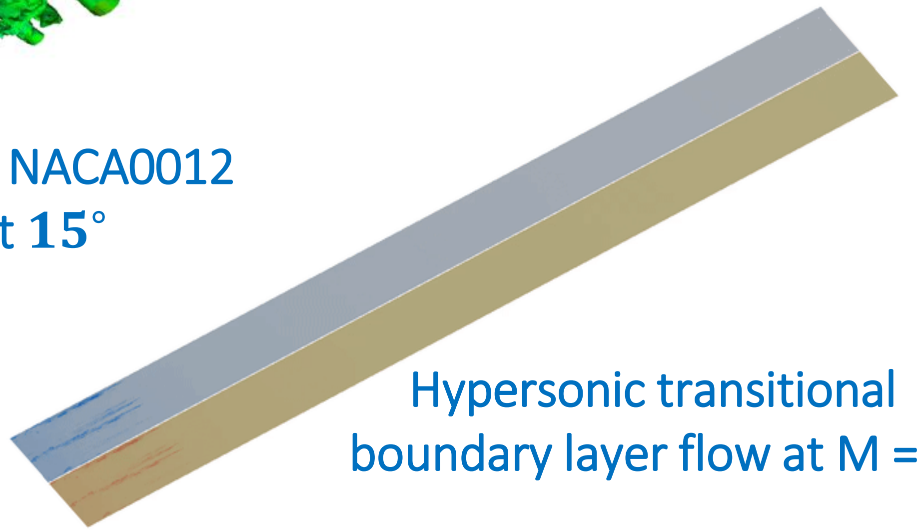

Hypersonic transitional boundary layer flow at M = 6

Total Grid Size	$\Delta x \times \Delta y \times \Delta z$	M_∞	Re_b
32M	$1.14\delta_0 \times 0.2\delta_0 \times 0.55\delta_0$	6	2.2×10^7

WMLES Simulations – Overview

Hypersonic Compression Ramp at M = 7.2

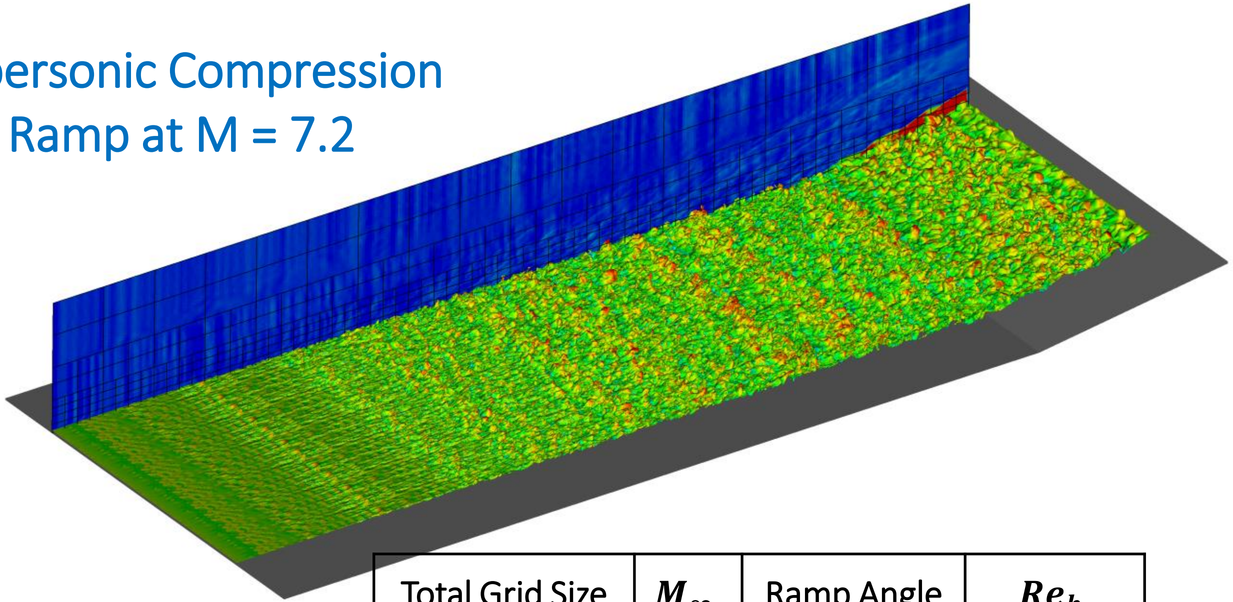

Total Grid Size	M_∞	Ramp Angle	Re_b
11M	7.2	8°	1.89×10^7

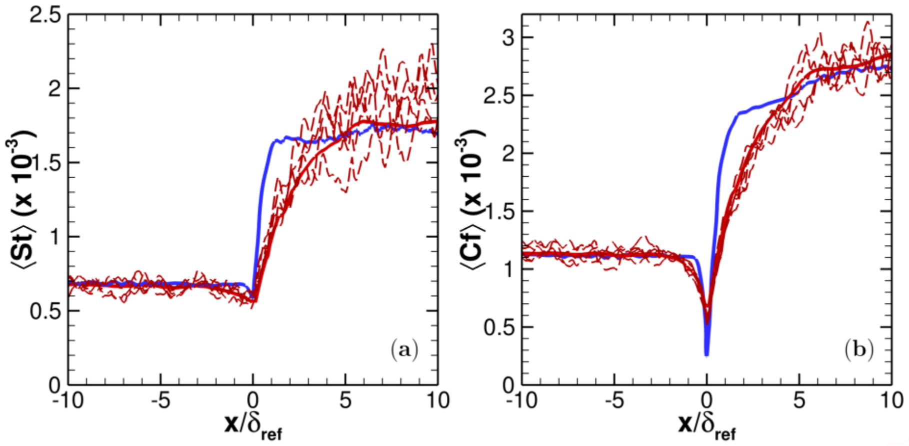

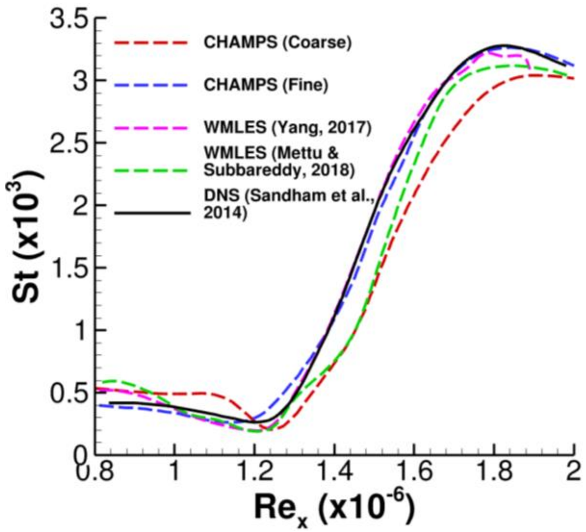

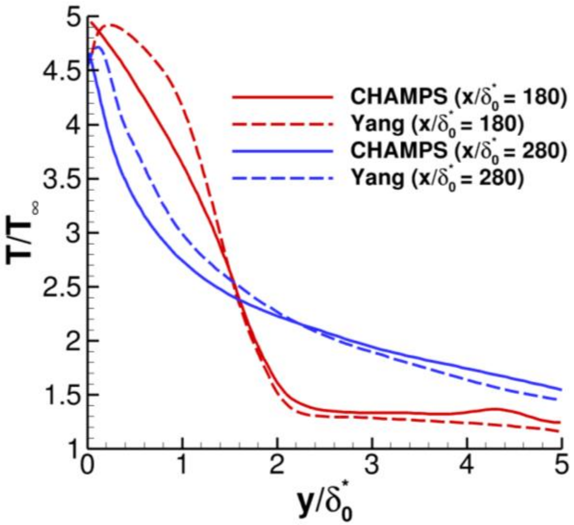

Shock-Wave Boundary-Layer Interaction at M = 6

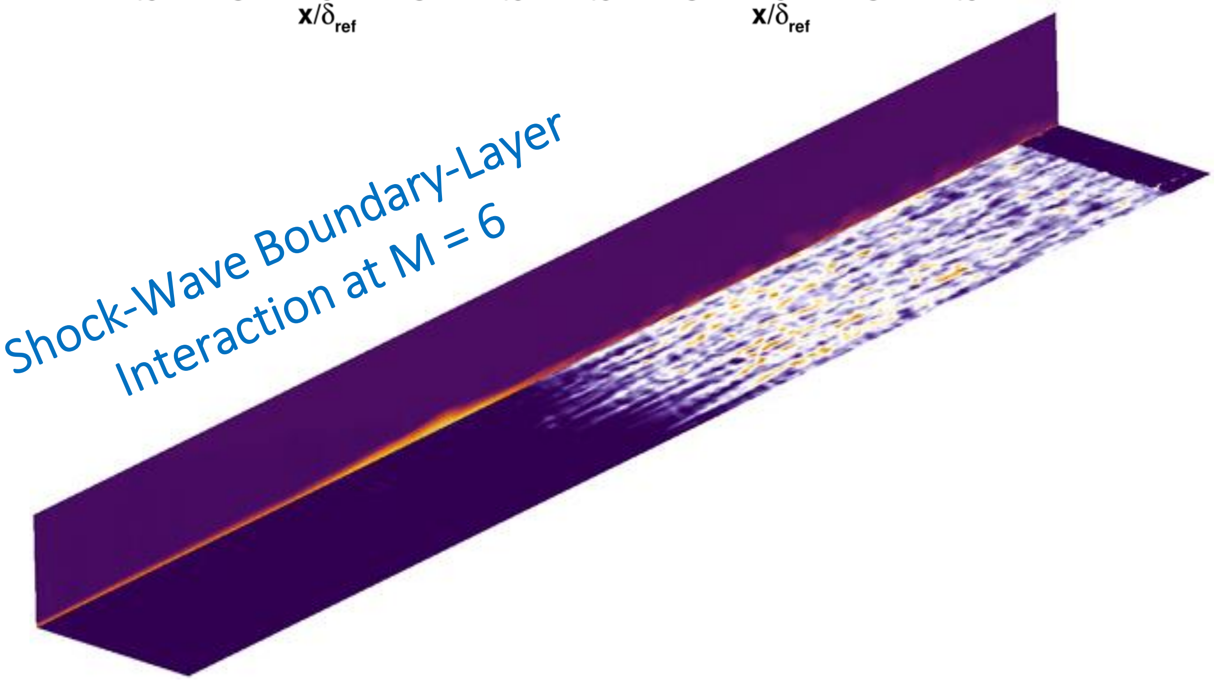

Total Grid Size	$\Delta x^+ \times \Delta y^+ \times \Delta z^+$	M_∞	Re_b
4.6M	$148 \times 50 \times 85$	6	6.0×10^6

WMLES Simulations – Turbulent Channel Flow

- Well-established test case in CFD community
- Skin friction Reynolds number $Re_\tau = 5200$
- Serves as basic validation case and development platform for interior schemes
- Initial condition is a perturbation at most amplified wavenumber (LST):

$$\Delta U(x, y, z) = \cos 2\pi z\,(\sin 2\pi x \sin 4\pi y + \sin 4\pi x \sin 8\pi y)$$

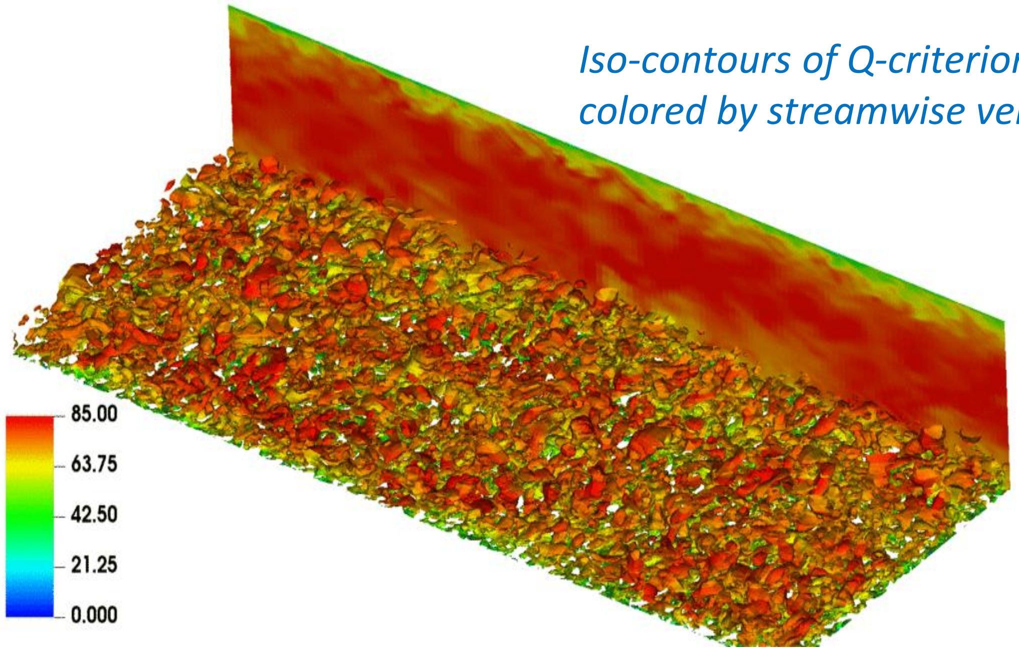

Iso-contours of Q-criterion colored by streamwise velocity

Grid topology for turbulent channel mesh

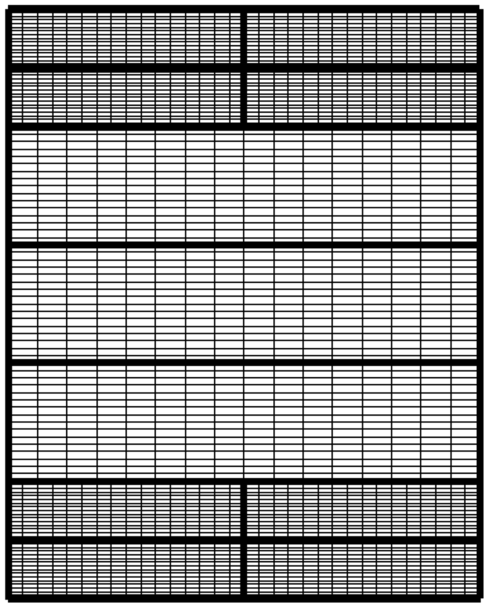

Total Grid Size	$\mathbf{\Delta x^+ \times \Delta y^+ \times \Delta z^+}$	$L_x \times L_y \times L_z$
1.9M	$270 \times 68 \times 270$	$12.8\delta \times 2\delta \times 4.8\delta$

WMLES Simulations – Turbulent Channel Flow

- Results demonstrate possibility of numerical artifacts near coarse-fine interface

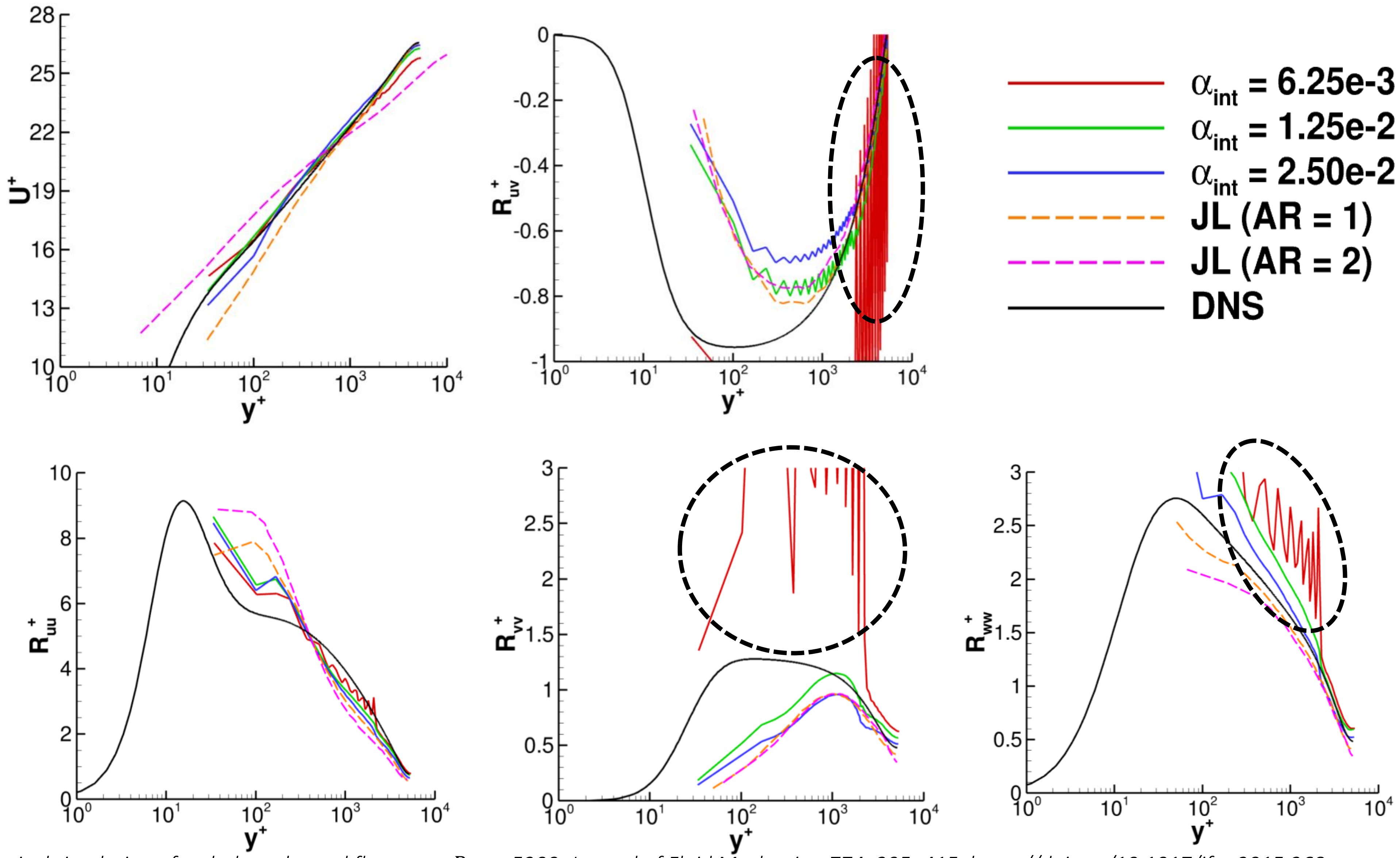

DNS: *Lee, M., & Moser, R. D. (2015). Direct numerical simulation of turbulent channel flow up to $Re_\tau \approx 5200$. Journal of Fluid Mechanics, 774, 395–415.* https://doi.org/10.1017/jfm.2015.268

JL: Wall-Modeled Large Eddy Simulation Resource: https://wmles.umd.edu

WMLES Simulations – Turbulent Channel Flow

- For low enough boundary dissipation coefficient, mean profile is invariant
- Reynolds stresses show dependence on the boundary dissipation term

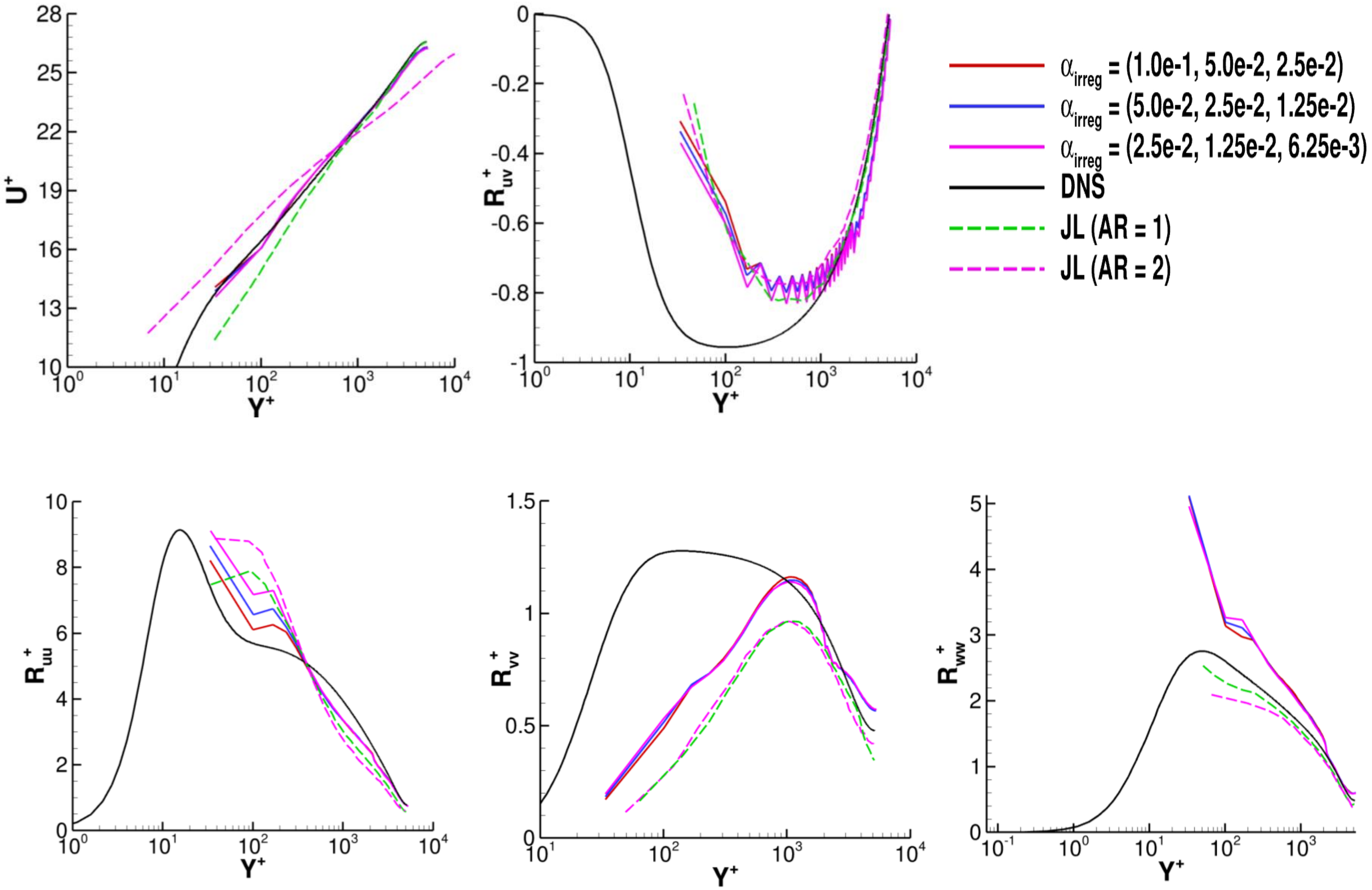

DNS: *Lee, M., & Moser, R. D. (2015). Direct numerical simulation of turbulent channel flow up to $Re_\tau \approx 5200$. Journal of Fluid Mechanics, 774, 395–415.* https://doi.org/10.1017/jfm.2015.268

JL: *Wall-Modeled Large Eddy Simulation Resource:* https://wmles.umd.edu

WMLES Simulations – M6 Transitional Boundary Layer

- Assess capability of IBM-WMLES to handle transitional flows
- Transition handled in the wall-model via the transition sensor, turbulent eddy viscosity suppressed in the wall model when below a prescribed threshold

$$T_r = 0.15\frac{\hat{\rho}\hat{k}}{\hat{\mu}|\hat{S}|}, \qquad k = \widehat{u_i u_i} - \hat{u}_i\hat{u}_i$$

- Promotion of transition via time-varying density perturbations

$$\rho' = \rho_\infty A W(y) \sum_{j=0}^{16} \cos\left(\frac{2\pi j z}{L_z} + \phi_j\right) \sum_{k=1}^{20} \sin(2\pi f_k t + \psi_k)$$

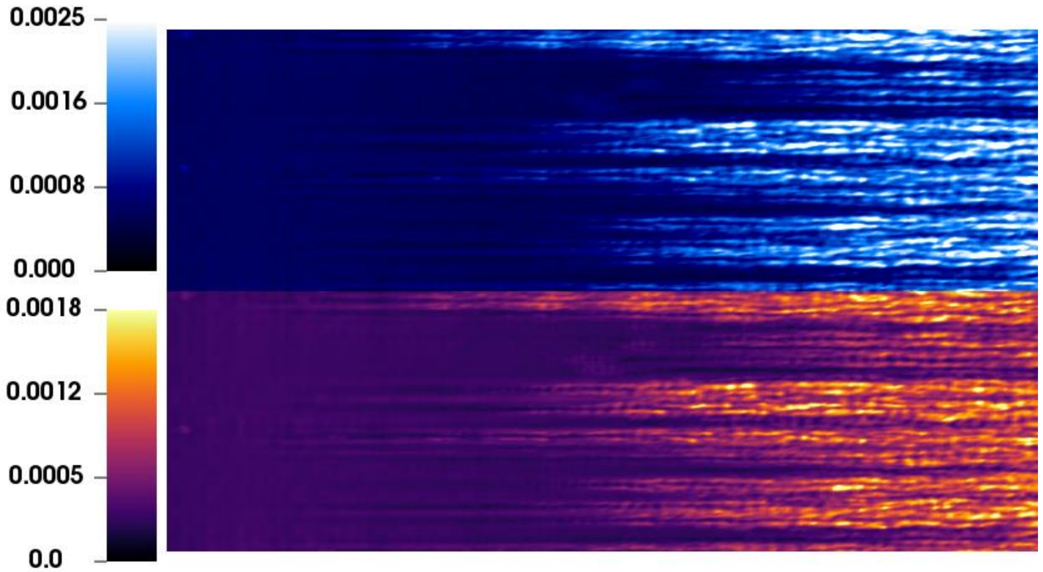

C_f (top) and St (bottom) on the flat-plate surface

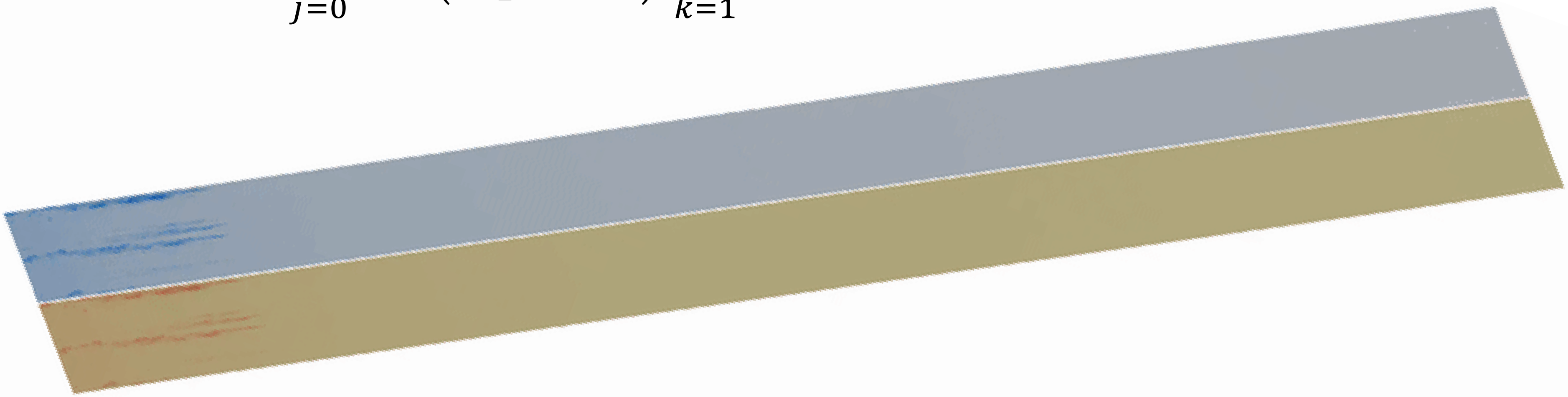

[1]Mettu, Subbareddy (2018), Wall modeled LES of compressible flows at non-equilibrium conditions, AIAA Aviation Forum

WMLES Simulations – M6 Transitional Boundary Layer

- Surface quantities are in good agreement with the reference DNS and WMLES simulations
- Effect of increasing transition sensor threshold is to delay transition

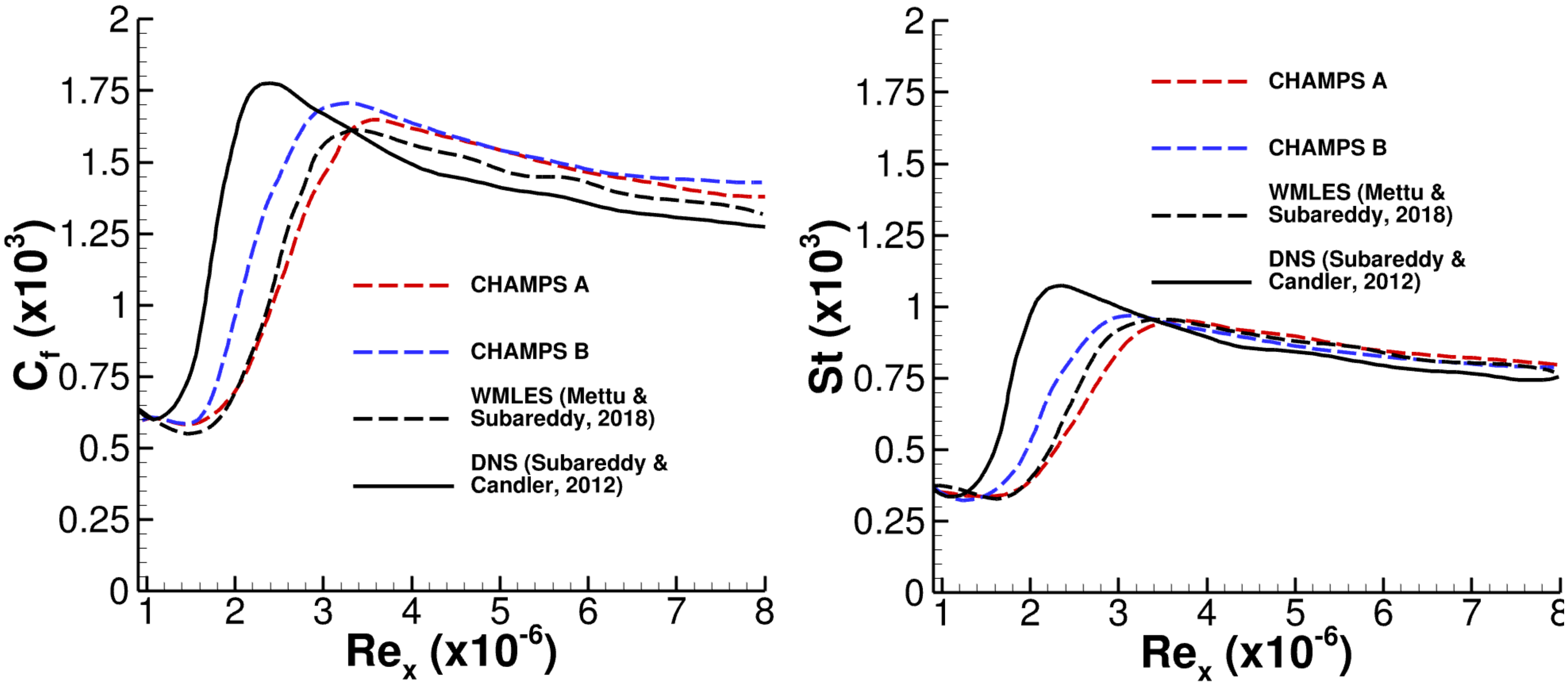

Skin friction (left) and Stanton number (right) for the M6 transitional boundary layer test case

WMLES Simulations – M6 Transitional SWBLI

- Test case has been the subject of a number of studies[1,2,3,…]
- Increase complexity over a simple boundary layer
- Presence of shock wave poses a challenge to the interior scheme
- Induced separation bubble introduces challenge of predicting point of separation
- Non-equilibrium effects present throughout the wall-model layer

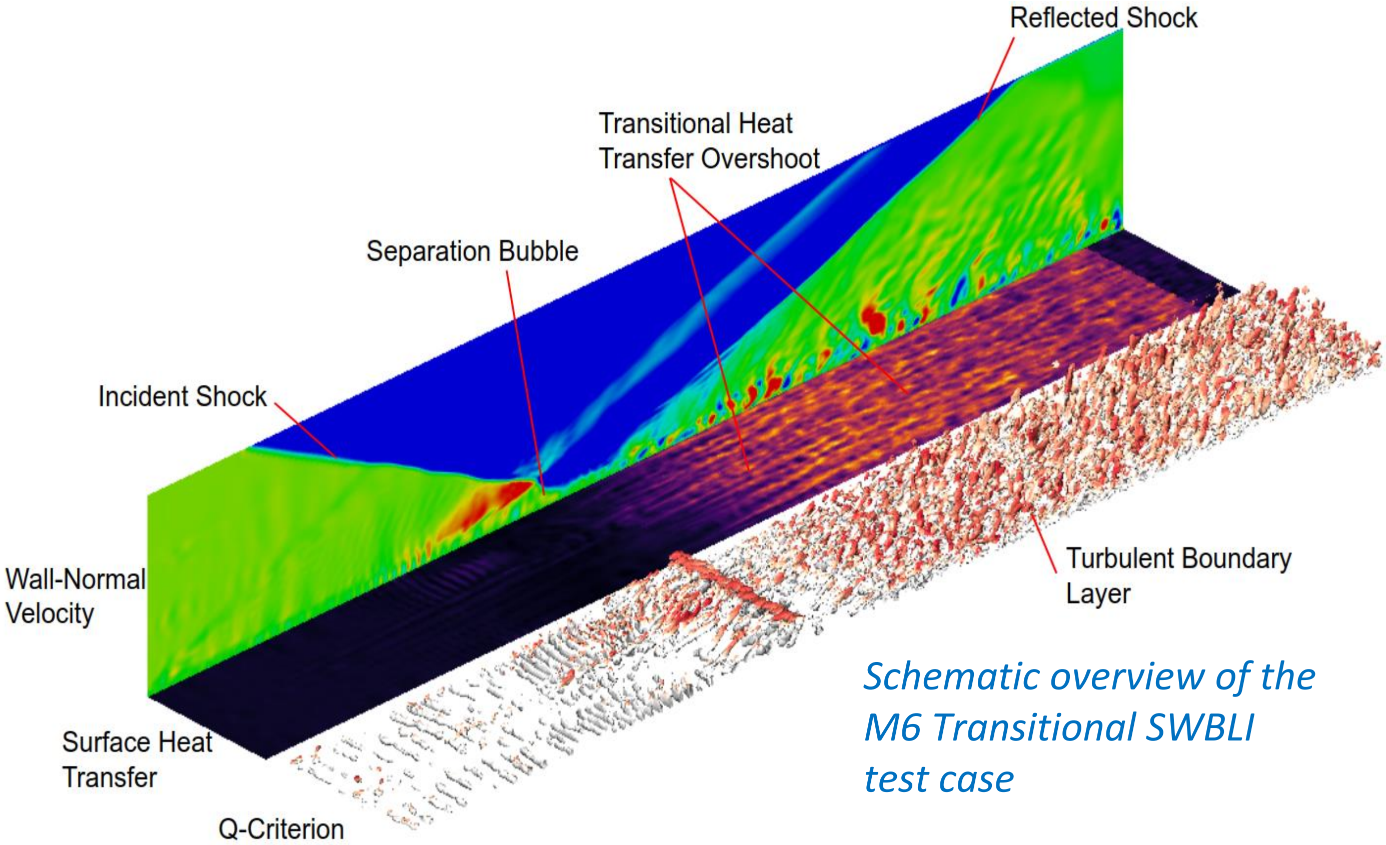

Schematic overview of the M6 Transitional SWBLI test case

[1] Sandham, N. D., Schülein, E., Wagner, A., Willems, S., & Steelant, J. (2014). "Transitional shock-wave/boundary-layer interactions in hypersonic flow". *Journal of Fluid Mechanics*, *752*, 349–382.
[2] Mettu, B. R., & Subbareddy, P. K. (2018). "Wall modeled LES of compressible flows at non-equilibrium conditions". In *2018 Fluid Dynamics Conference*. American Institute of Aeronautics and Astronautics.
[3] Ganju, S., van Noordt, W., & Brehm, C. (2021). "Progress in the Development of an Immersed Boundary Viscous-Wall Model for 3D and High-Speed Flows". In *AIAA Scitech 2021 Forum*.

WMLES Simulations – M6 Transitional SWBLI

- Overall, good agreement in surface quantities with the DNS and WMLES references
- Temperature profile mismatch – possibly due to difference in the energy equation coupling
- Coarser grid resolution under-predicted separation length, peak heat transfer

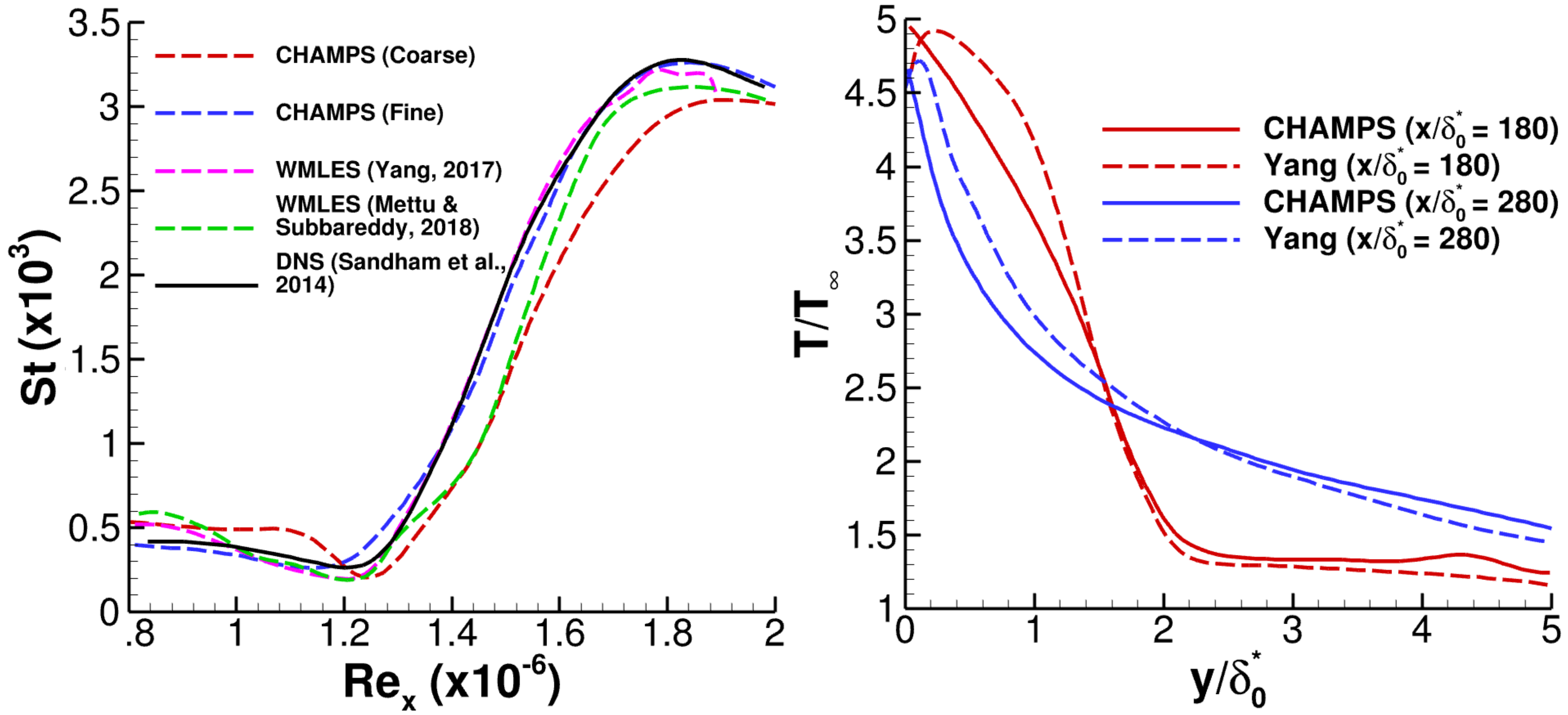

Stanton number (left) and temperature profile (right) for the M6 SWBLI test case

WMLES Simulations – M6 Transitional SWBLI

- A test was run to investigate the effect of boundary dissipation for this test case
- Coarse mesh
- Significant effect of boundary dissipation term
- Dissipation coefficient manipulated only in the first three grid cells
- Effect of dissipation apparently more significant than order-of-accuracy beyond 4th order

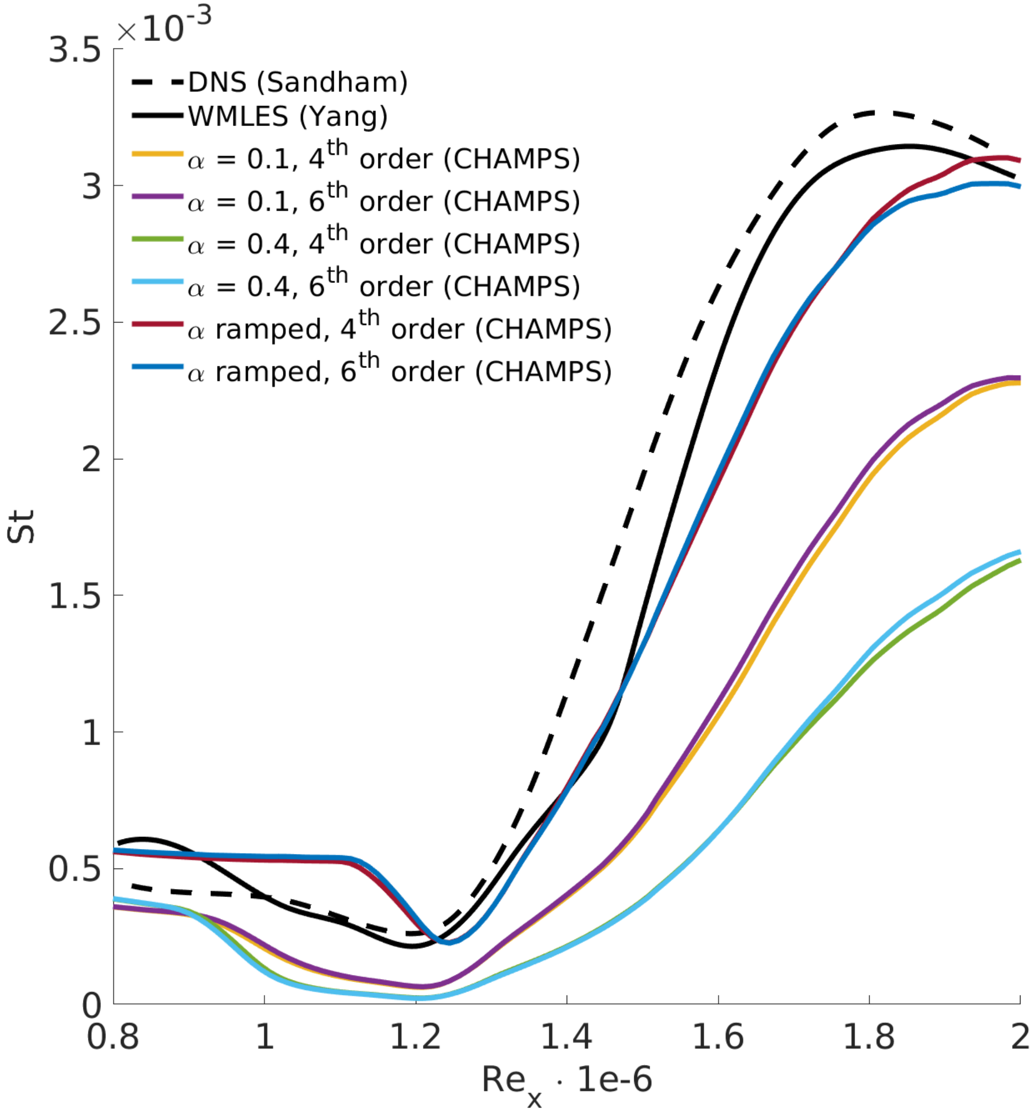

Stanton number predictions showing variations of dissipation coefficient at the immersed boundary

WMLES Simulations – SWBLI

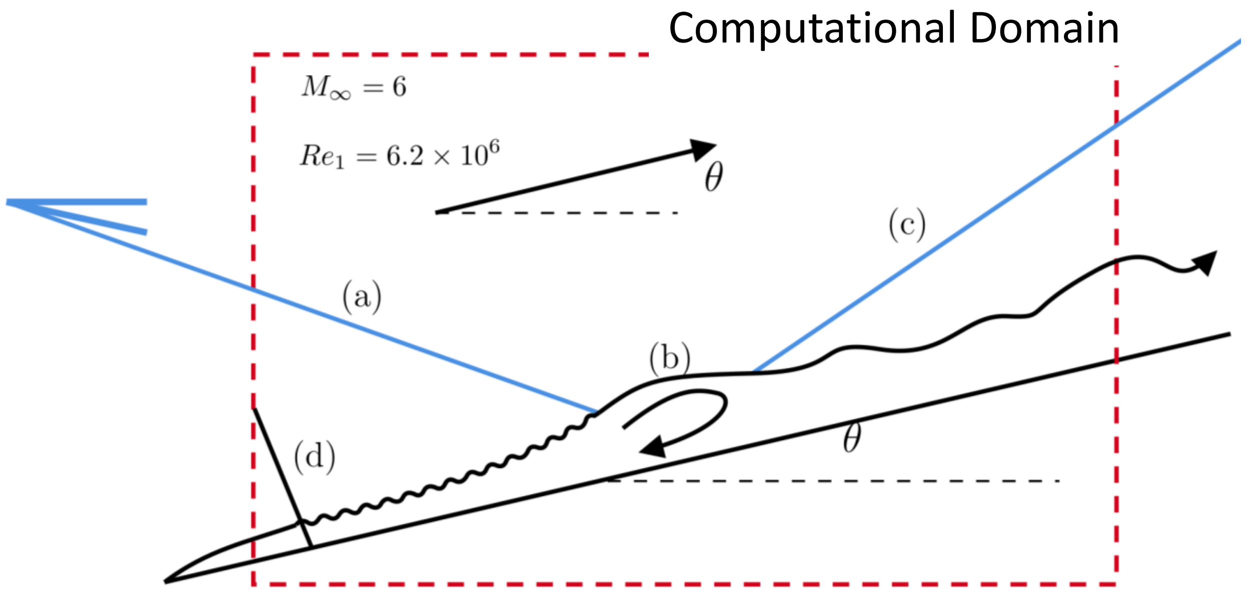

Schematic of the SWBLI ramp test-case: (a) incoming shock wave, (b) induced separation bubble, (c) reflected shock wave, and (d) density disturbances.

Flow visualization for the inclined SWBLI case at an angle of 12 degrees. Surface: skin friction. Rear plane: temperature contours

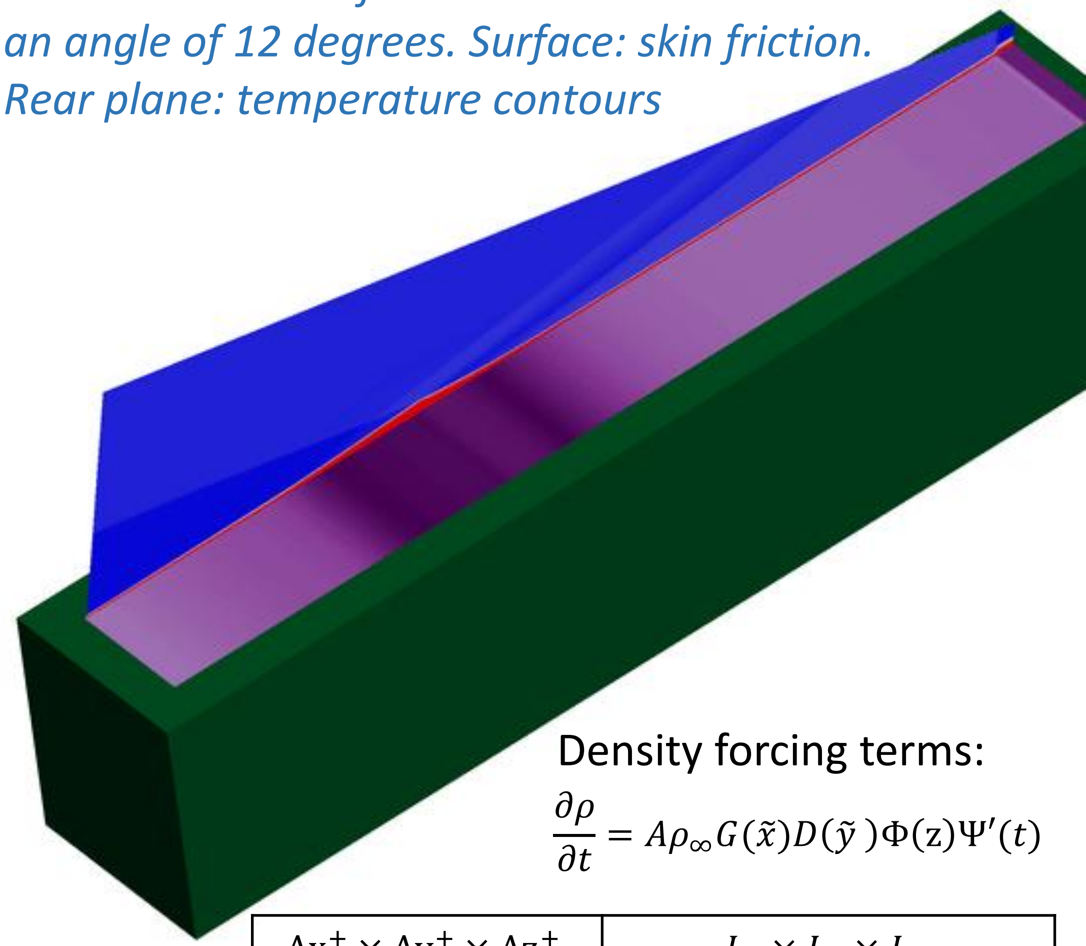

- To test IB treatment, an angle of inclination is introduced
- Shock wave at inflow imposed via Rankine-Hugoniot relations
- Impingement of shock wave induces a separation bubble
- Present method has been validated previously for grid aligned variation[3]

Density forcing terms:

$$\frac{\partial \rho}{\partial t} = A\rho_\infty G(\tilde{x})D(\tilde{y})\Phi(z)\Psi'(t)$$

$\Delta x^+ \times \Delta y^+ \times \Delta z^+$	$L_x \times L_y \times L_z$
$41 \times 40 \times 120$	$381\delta_0 \times 91\delta_0 \times 47\delta_0$

WMLES Simulations – SWBLI

- Grid alignment was briefly analyzed to assess suitability of fixed grid spacing for varying angle of inclination
- Unit aspect ratio gives small variation in the dependence of numerical errors on angle of inclination
- Variation of numerical errors less significant when avoiding inclinations near various critical angles

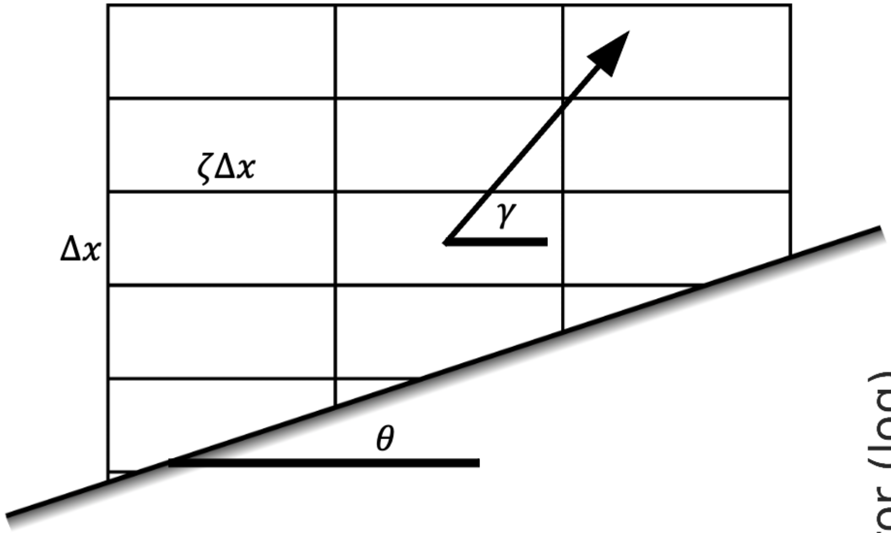

Significant parameters in understanding the effect of grid alignment on solution accuracy

Phase Error

$$\epsilon_p = \left\| \frac{u}{Du} - \frac{u}{\widehat{D}u} \right\|$$

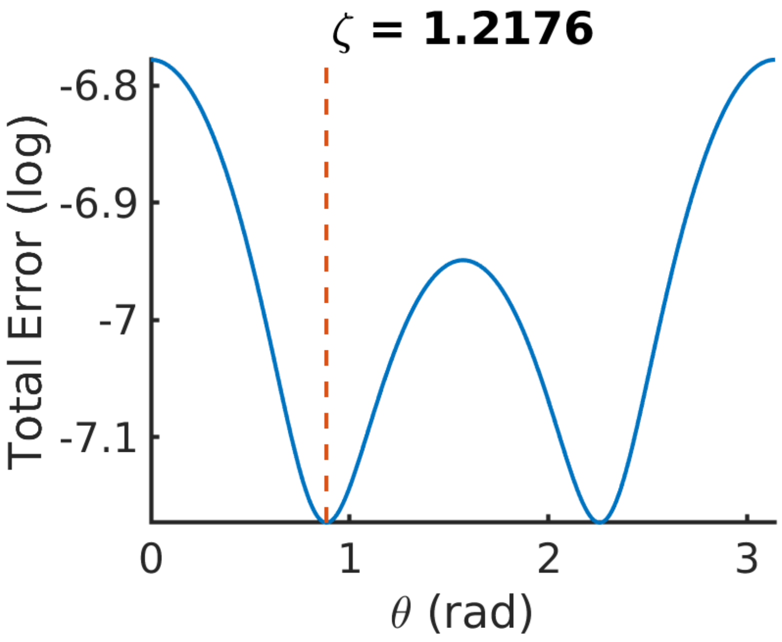

Truncation Error

$$\epsilon_t = \frac{1}{\Delta x^{2n+1}} \left\| Du - \widehat{D}u \right\|$$

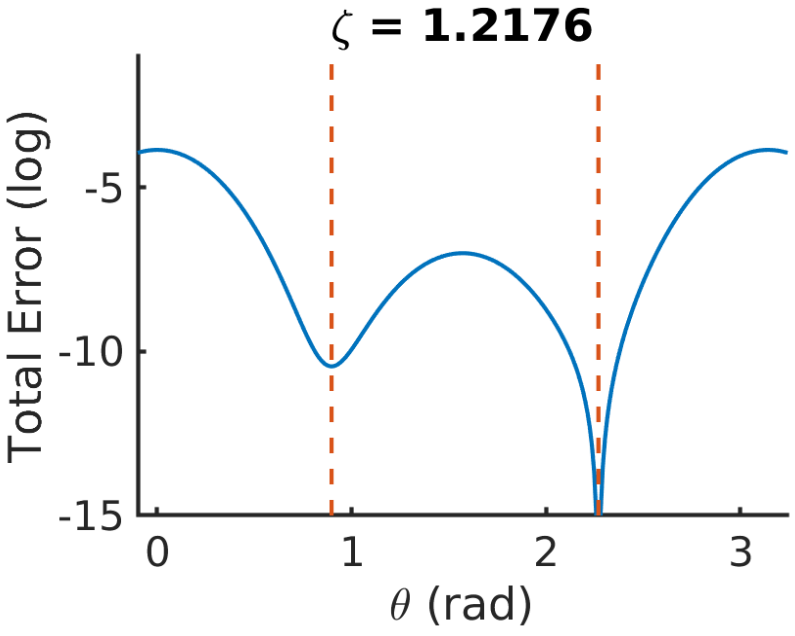

WMLES Simulations – SWBLI

Computational Domain

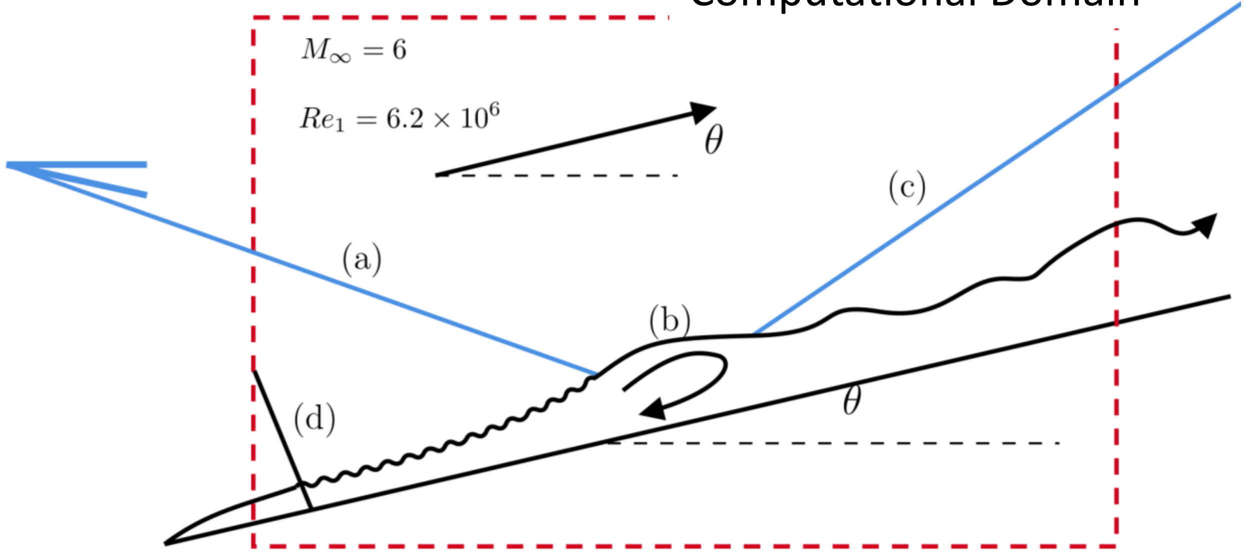

Schematic of the SWBLI ramp test-case: (a) incoming shock wave, (b) induced separation bubble, (c) reflected shock wave, and (d) density disturbances.

Stanton Number

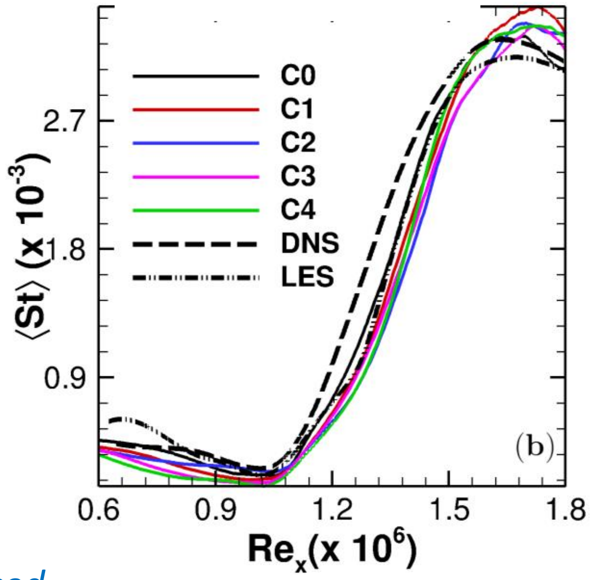

Pressure Distribution

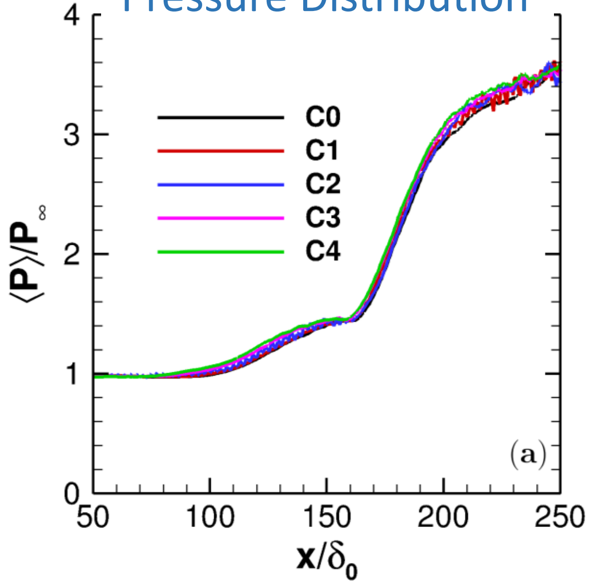

Tangential Velocity

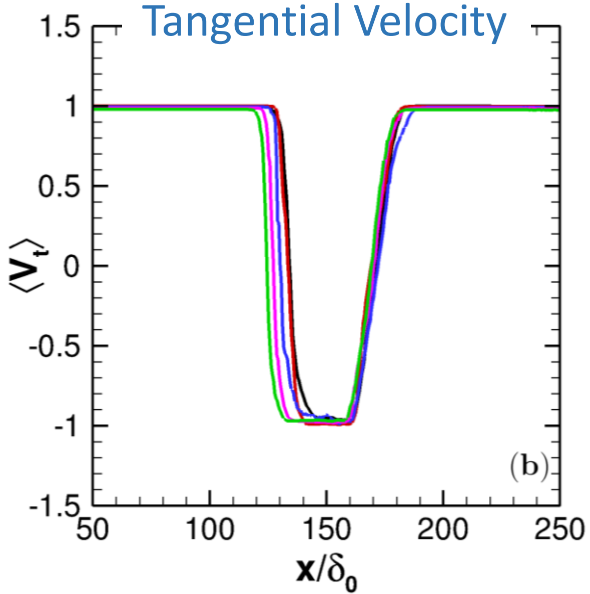

- Good agreement in peak turbulent/transitional heat transfer among all angles of inclination
- Consistency in surface pressure prediction
- Mean separation location indicated by the time- and space-averaged streamwise component of normalized velocity at wall
- Small disagreement ($\approx 8\delta_0$) in separation location

WMLES Simulations – SWBLI

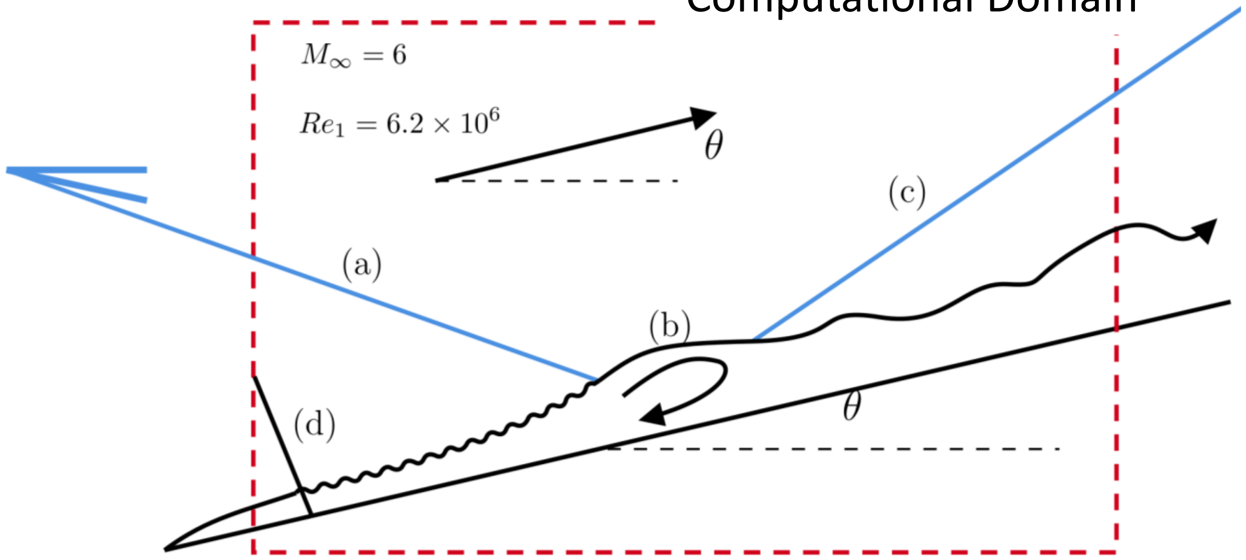

Schematic of the SWBLI ramp test-case: (a) incoming shock wave, (b) induced separation bubble, (c) reflected shock wave, and (d) density disturbances.

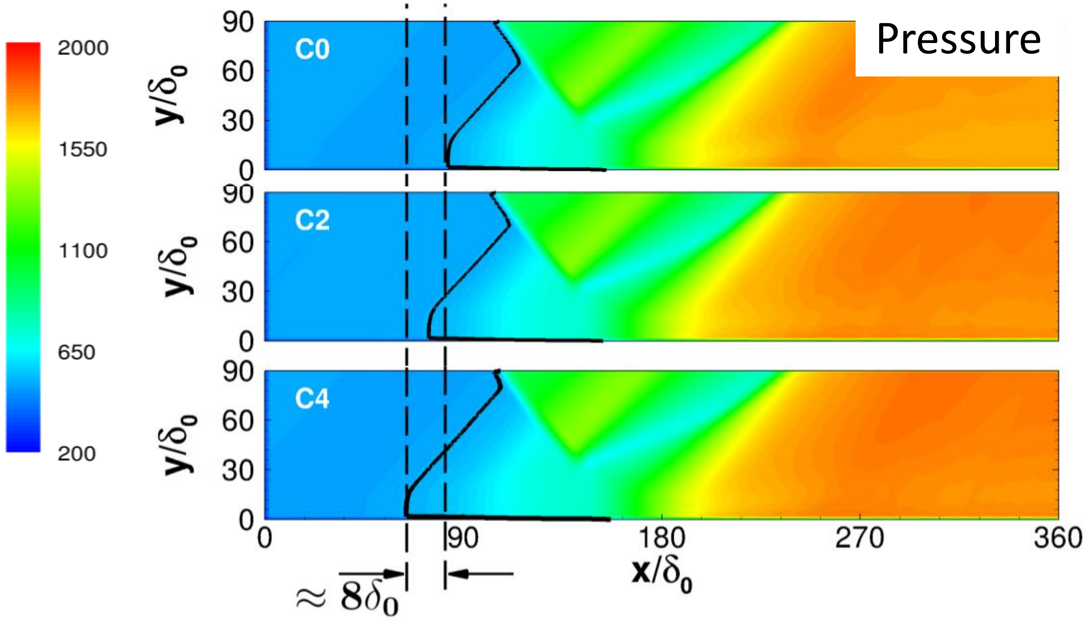

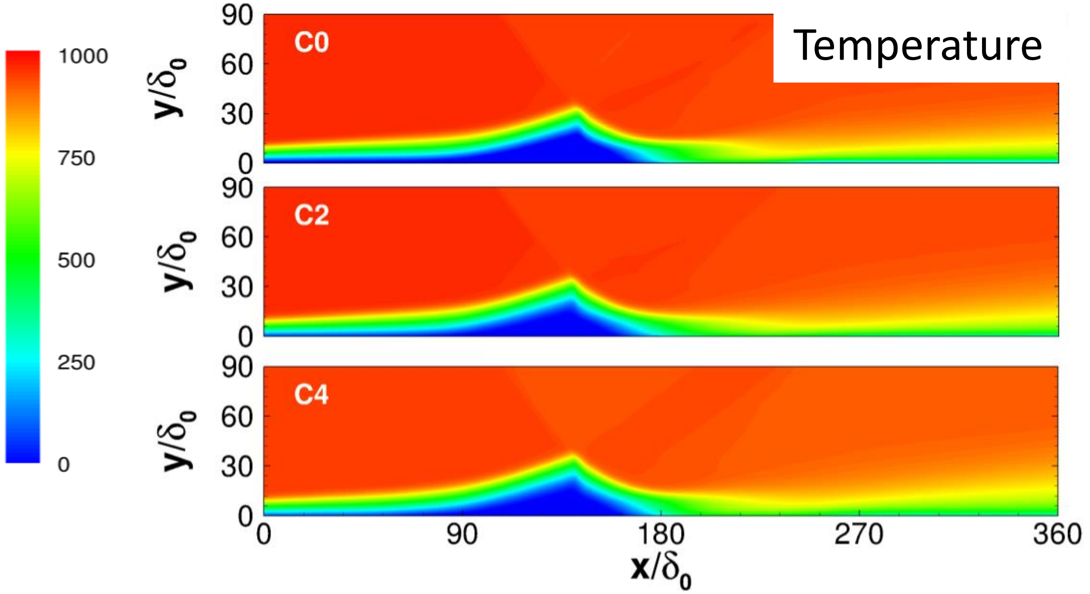

- Good agreement in peak turbulent/transitional heat transfer among all angles of inclination
- Consistency in surface pressure prediction
- Mean separation location indicated by the time- and space-averaged streamwise component of normalized velocity at wall
- Small disagreement ($\approx 8\delta_0$) in separation location

WMLES Simulations – SWBLI

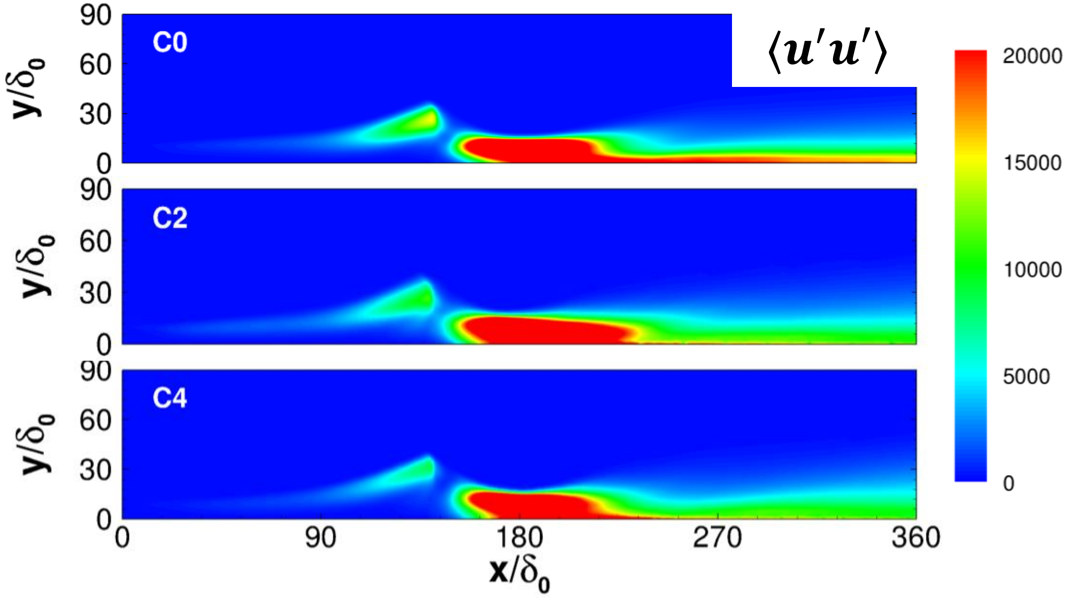

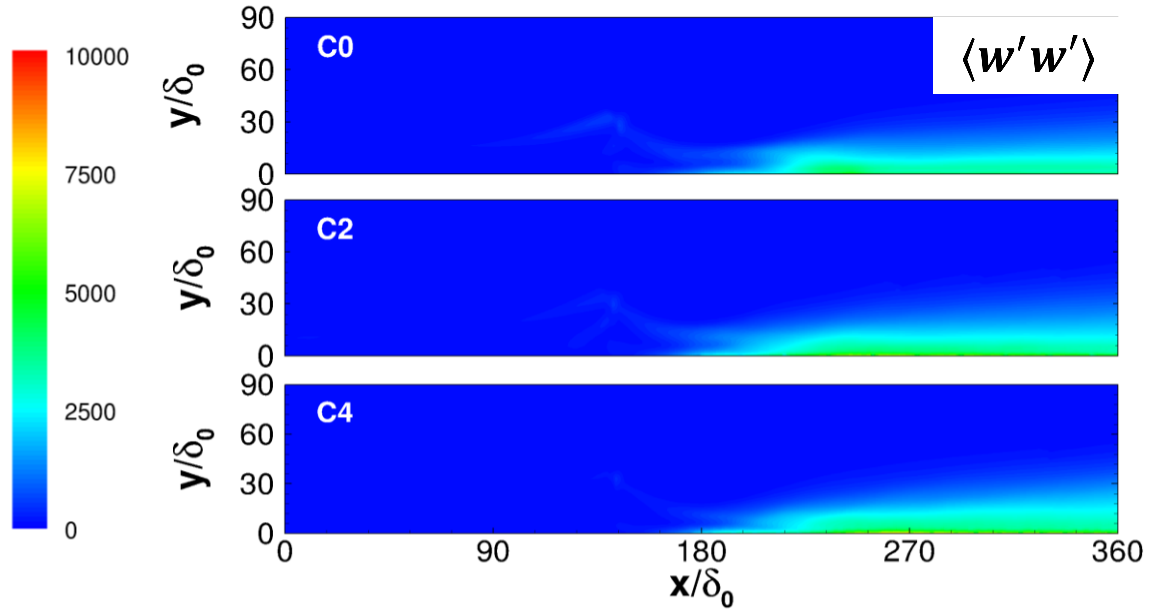

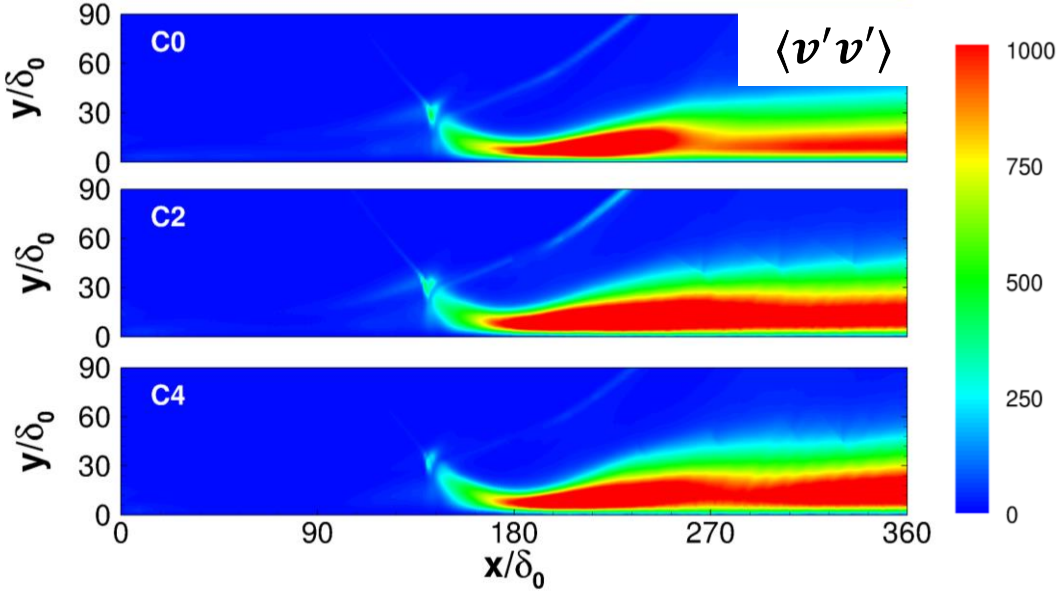

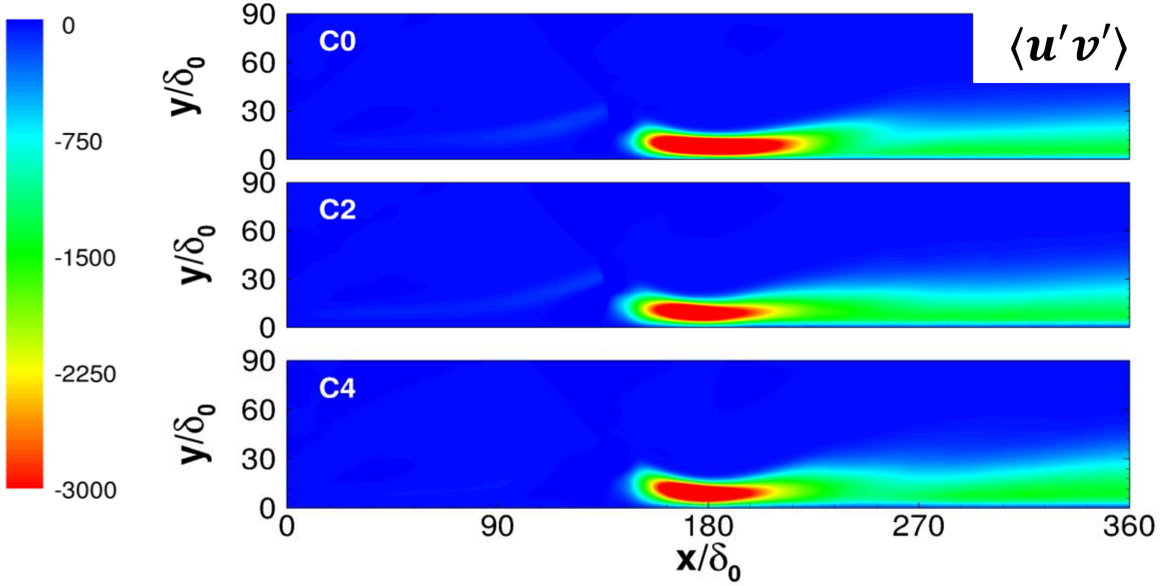

WMLES Simulations – Compression Corner

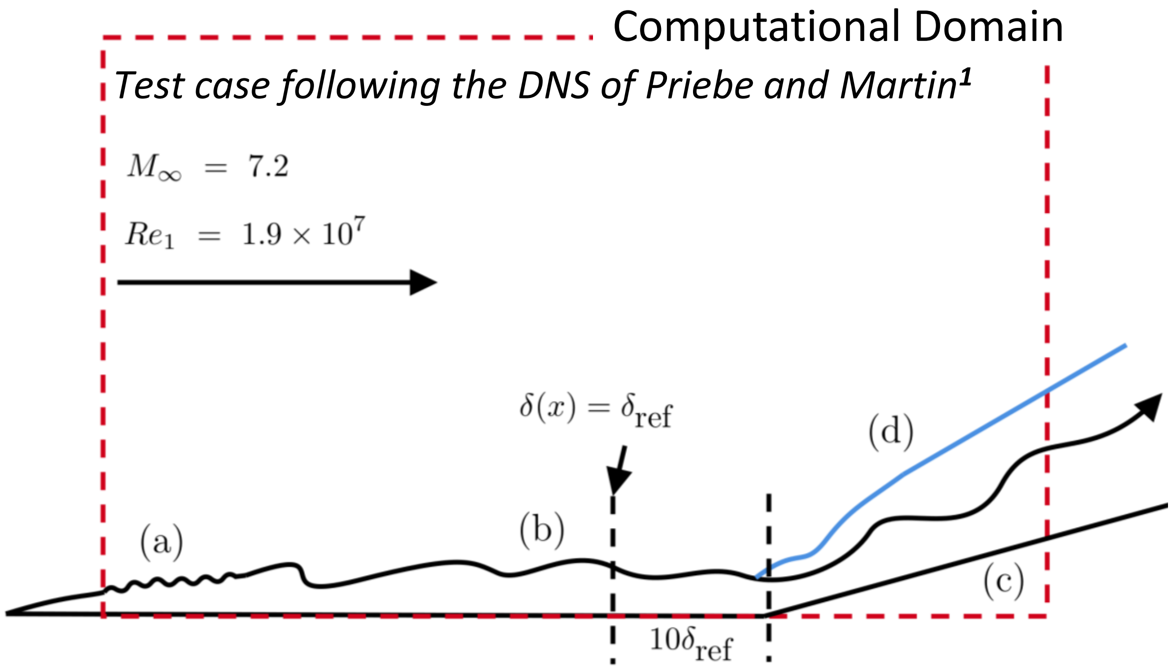

Schematic of the compression ramp test-case. (a) Density disturbances, (b) turbulent boundary layer, (c) 8° compression ramp, and (d) induced shock wave

Flow visualization for the compression ramp test case. Contours of heat flux and temperature in rear plane

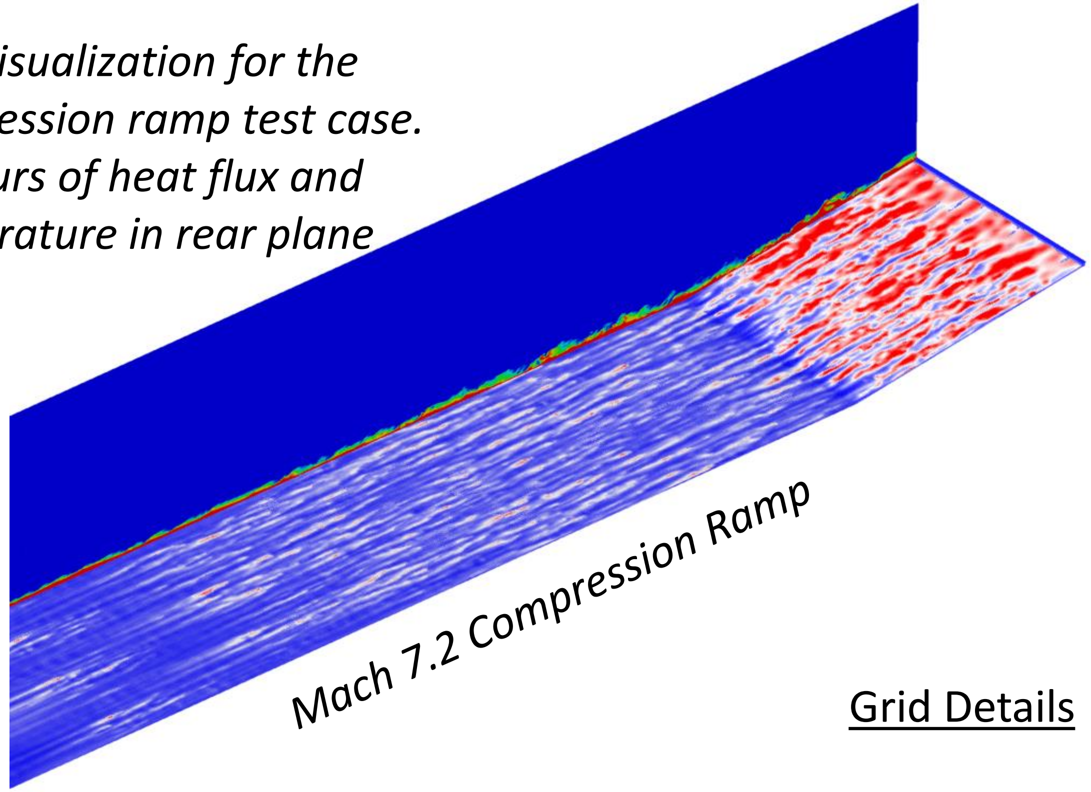

- Freestream-to-wall temperature ratio of 0.185
- Spatially, ~5% cost of the reference DNS (WMLES 11M, DNS 235M)

<u>Grid Details</u>

	$\Delta x^+ \times \Delta y^+ \times \Delta z^+$	$L_x \times L_y \times L_z$
Coarse	$160 \times 80 \times 190$	$68\delta_{ref} \times 9\delta_{ref} \times 10\delta_{ref}$
Fine	$90 \times 40 \times 110$	$68\delta_{ref} \times 9\delta_{ref} \times 10\delta_{ref}$

WMLES Simulations – Compression Corner

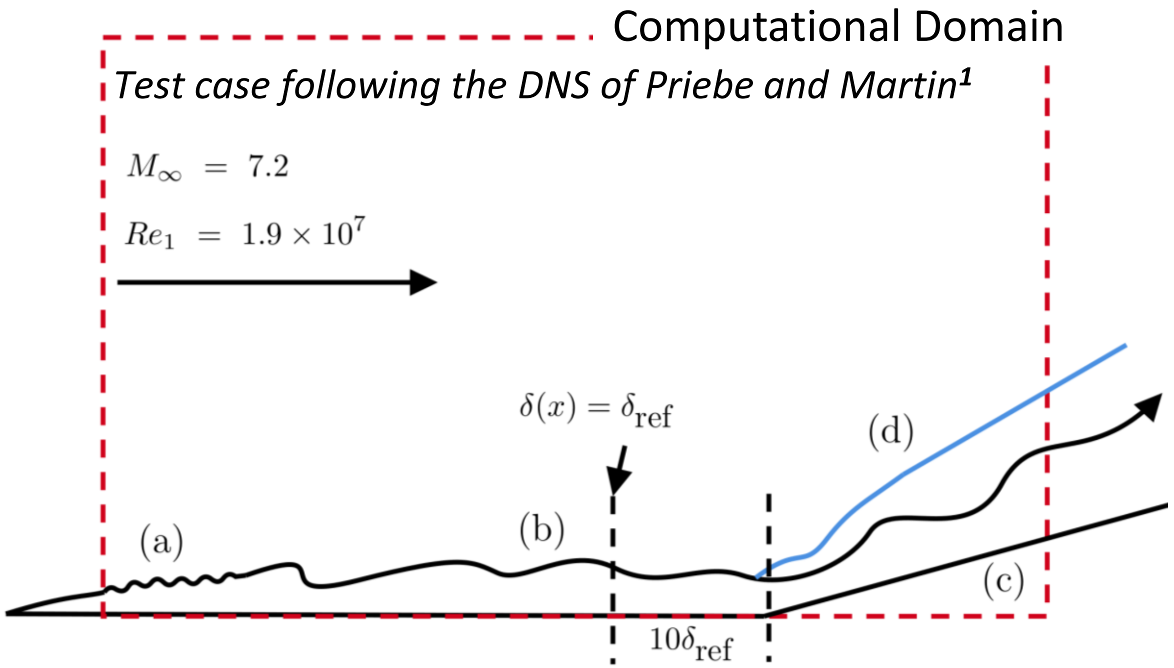

Schematic of the compression ramp test-case. (a) Density disturbances, (b) turbulent boundary layer, (c) 8° compression ramp, and (d) induced shock wave

Stanton Number

Skin Friction

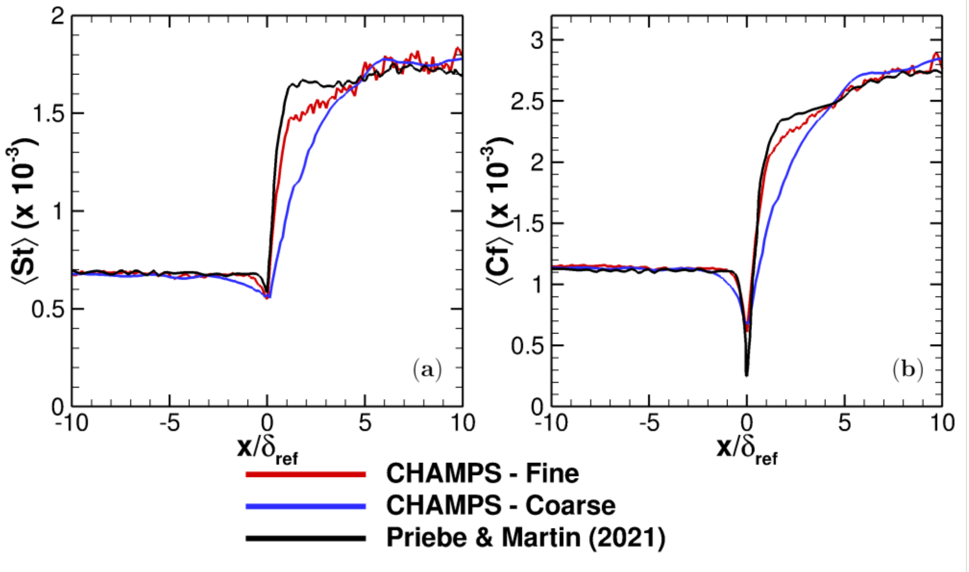

Pressure Distribution

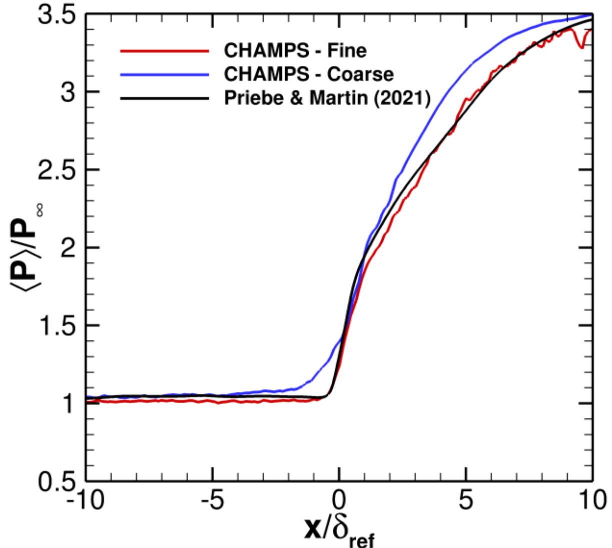

- Flow remains attached in the mean, but significant instantaneous separation
- Present IB treatment remained stable through transition, as well as at the corner location
- Ramp geometry not aligned with the Cartesian grid
- Equilibrium assumptions appear to break down at the corner location

Future Work

- Move towards complex, practical geometries
- Non-equilibrium wall modeling and wall-modeling for laminar flows
- High-enthalpy and chemical non-equilibrium flows

AIAA Smooth-Body Separation Workshop (AIAA SciTech 2022)

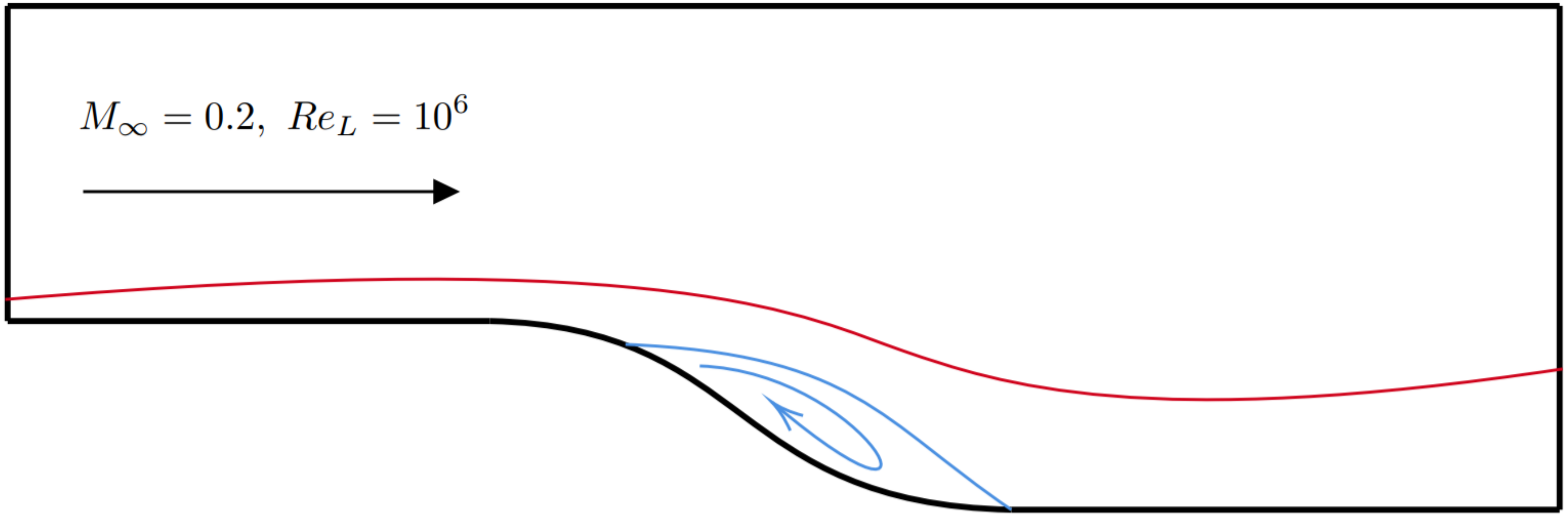

Schematic diagram for smooth-body flow separation test case

- To be held at SciTech 2022
- Understanding various effects on smooth-body separation
- Not too late to participate!
- wmles.umd.edu

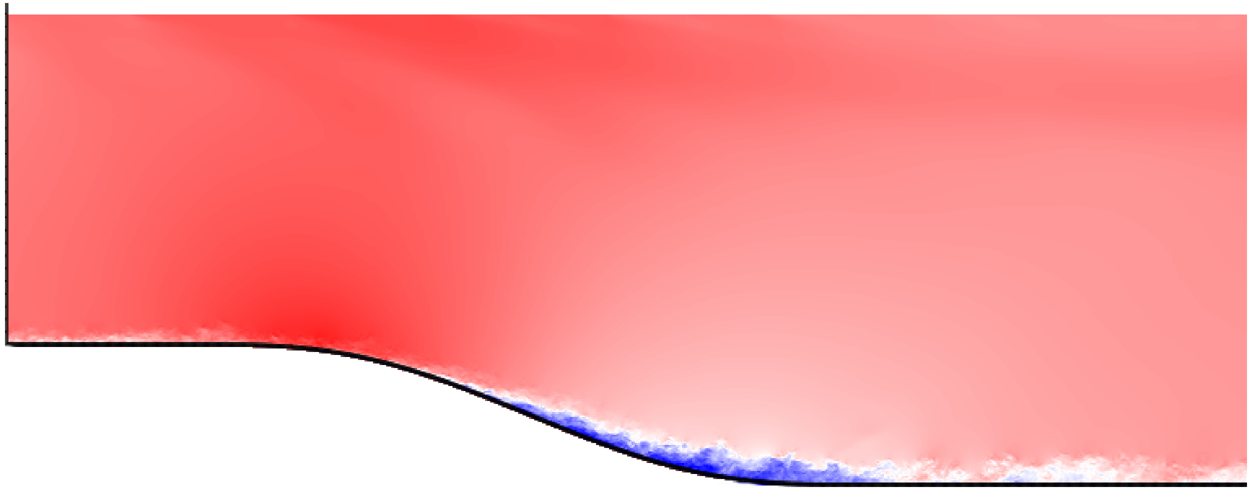

Preliminary calculation for smooth-body flow separation test case

Thank you!

Any Questions?